Elevated expression of complement C4 in the mouse prefrontal cortex causes schizophrenia-associated phenotypes

Mélanie Druart, Marika Nosten-Bertrand, Stefanie Poll, Sophie Crux, Felix Nebeling, Célia Delhaye, Yaëlle Dubois, Manuel Mittag, Marion Leboyer, Ryad Tamouza, et al.

Elevated expression of complement C4 in the mouse prefrontal cortex causes schizophrenia-associated phenotypes

Running title: Elevated C4 causes schizophrenia-like phenotypes

Mélanie Druart[1,2,3], Marika Nosten-Bertrand[1,2,3*], Stefanie Poll[4*], Sophie Crux[4*], Felix Nebeling[4*], Célia Delhaye[1,2,3], Yaëlle Dubois[1,2,3], Manuel Mittag[4], Marion Leboyer[5,6], Ryad Tamouza[5,6], Martin Fuhrmann[4], Corentin Le Magueresse[1,2,3#]

[1]INSERM UMR-S 1270, 75005 Paris, France
[2]Sorbonne Université, 75005 Paris, France
[3]Institut du Fer à Moulin, 17 rue du Fer à Moulin, 75005 Paris, France
[4]Neuroimmunology and Imaging Group, German Center for Neurodegenerative Diseases, 53175 Bonn, Germany
[5]INSERM U955, Neuro-Psychiatrie Translationnelle, Université Paris-Est, Créteil, France.
[6]AP-HP, DMU IMPACT, Département Médical Universitaire de Psychiatrie, Hôpitaux Universitaires Henri Mondor, Créteil, France.

* Equal contribution
# Correspondence: corentin.le-magueresse@inserm.fr

Abstract

Accumulating evidence supports immune involvement in the pathogenesis of schizophrenia, a severe psychiatric disorder. In particular, high expression variants of *C4*, a gene of the innate immune complement system, were shown to confer susceptibility to schizophrenia. However, how elevated C4 expression may impact brain circuits remains largely unknown. We used *in utero* electroporation to overexpress C4 in the mouse prefrontal cortex (PFC). We found reduced glutamatergic input to pyramidal cells of juvenile and adult, but not of newborn C4-overexpressing (C4-OE) mice, together with decreased spine density, which mirrors spine loss observed in the schizophrenic cortex. Using time-lapse two-photon imaging *in vivo*, we observed that these deficits were associated with decreased dendritic

spine gain and elimination in juvenile C4-OE mice, which may reflect poor formation and/or stabilization of immature spines. In juvenile and adult C4-OE mice we found evidence for NMDA receptor hypofunction, another schizophrenia-associated phenotype, and synaptic accumulation of calcium-permeable AMPA receptors. Alterations in cortical GABAergic networks have been repeatedly associated with schizophrenia. We found that functional GABAergic transmission was reduced in C4-OE mice, in line with diminished GABA release probability from parvalbumin interneurons, lower GAD67 expression and decreased intrinsic excitability in parvalbumin interneurons. These cellular abnormalities were associated with working memory impairment. Our results substantiate the causal relationship between an immunogenetic risk factor and several distinct cortical endophenotypes of schizophrenia, and shed light on the underlying cellular mechanisms.

Introduction

Genome-wide association studies (GWAS) identified genes involved in immune and in autoimmune processes that are associated with Schizophrenia (SZ)[1-4]. The major GWAS locus in SZ lies within the major histocompatibility complex (MHC) locus on chromosome 6[4]. This includes the *C4* gene which consists of *C4A* and *C4B* gene copy number variations and insertion/deletion of the human endogenous retrovirus K (HERVK). A detailed analysis of this locus showed a strong relationship between the genetic diversity of the C4 region and SZ[5]. In particular, the presence of several copies of *C4A* with HERVK insertions correlated with higher *C4A* expression and increased risk of SZ. The complement pathway is a central determinant of synaptic pruning, a developmental process in which the synaptic connections between neurons are refined in the brain from childhood until early adulthood[6]. Thus, the identification of *C4A* as a risk factor in SZ established a link between complement-mediated synaptic pruning and dendritic spine loss in the cortex of schizophrenic patients, a characteristic feature of the disease which had long been hypothesized to reflect excessive synapse refinement in adolescence[7, 8].

In mice, the *C4b* gene presents homology with both the *C4A* and *C4B* genetic motifs of the human *C4* gene locus. Connectivity between the retina and the visual thalamus is impaired in C4 knock-out mice[5], indicating that the mouse C4 protein participates in synaptic pruning. It has been hypothesized that high C4 expression may result in increased synaptic pruning in upper layers of the neocortex[5]. Indeed *C4A* and *C4B* gene copy numbers positively correlated with neuropil contraction, which is often considered as a mesoscale correlate of

developmental synapse elimination[9]. *C4A* gene copy numbers are associated with increased neuronal complement deposition and microglial synapse uptake in co-cultures of human iPSC-derived neurons and microglial cells[10]. Furthermore, it was shown that elevated C4 expression in the mouse prefrontal cortex causes dendritic spine loss, increased engulfment of synaptic material by microglial cells and impaired social behaviors[11]. A recently published study also showed that mice overexpressing human C4A display reduced cortical synapse density, increased microglial engulfment of synapses and altered social behavior, anxiety levels and spatial short-term memory[12].

In addition to spine loss, several neural endophenotypes have been identified in the cortex of schizophrenic patients. Decreased NMDA receptor (NMDAR)-mediated neurotransmission in SZ has been inferred from at least four lines of evidence[13]: i) NMDAR antagonists induce schizophrenic-like behaviors; ii) the expression of NMDAR subunits is reduced in post-mortem brain tissue from schizophrenic patients iii) auto-antibodies against NMDA receptors cause clinical symptoms of SZ; iv) *GRIN2A*, an NMDAR subunit-encoding gene, has been associated with SZ in recent GWAS. Moreover, multiple deficits in GABAergic circuits have been identified in SZ. Abnormalities in GABAergic networks include reduced GABA concentration in the brain of schizophrenic patients, decreased expression of GAD67, an enzyme responsible for GABA synthesis, and abnormalities at parvalbumin-expressing (PV) neuron-pyramidal cell synapses[14]. What causes these distinct alterations, and how they relate to each other, is poorly understood. The relationship between C4 and SZ-associated cortical endophenotypes such as reduced NMDA receptor-mediated transmission, loss of GAD67 expression and altered GABAergic synapses remains unknown.

Here we examined the consequences of complement C4 overexpression in layer II/III pyramidal cells of the mouse prefrontal cortex on neuronal circuit development and function. C4 overexpression recapitulated several cortical phenotypes that have been associated SZ, including decreased spine number and reduced NMDA receptor function in pyramidal cells. Intriguingly, dendritic spine loss was accompanied by decreased spine turnover in juvenile mice. We also report several abnormalities in GABAergic circuits in C4-OE mice which are consistent with the alterations of GABAergic markers seen in the brain of SZ patients. Finally, our results reveal that the selective overexpression of C4 in PFC layer II/III is sufficient to impair working memory, which is reminiscent of SZ-associated cognitive deficits.

Methods

A brief summary of experimental procedures is provided here with additional details available in the Supplemental Information accompanying this article. Additionally, Supplementary Tables S1-4 provide an overview of the number of recordings, animals and statistics in the different experiments.

Animals

All animal experiments were performed according to guidelines of the European Community for the use of animals in research and were approved by the local ethical committees (C2EA-05 in France; LANUV NRW in Germany). All experiments were performed on mice that had been electroporated at embryonic stage E15 and were on a C57Bl/6J background.

In utero electroporation

Pregnant mice at E15 were anesthetized by isoflurane 4% and were injected with Flunixin (0.05 mg/kg body weight) before surgery. The surgery was performed under isoflurane 2% on a heated blanket and breathing was carefully monitored during all the procedure.

Between 0.5 µl to 1µl of a solution containing pCAG-C4HA vector (0.8 µg/µl) together with pCAG-TdTomato vector (0.4 µg/µl) (molar ratio 4:1) in NaCl 0.9% were injected into the bilateral ventricles. In the control condition, a solution containing pCAG-TdTomato (0.8 µg/µl) alone was injected. Electrical pulses (50V; 50 ms) were applied five times at intervals of 950 ms with an electroporator (see Supplementary Information).

In vivo two-photon imaging

Two-photon imaging was performed right after surgery at a Zeiss 7 multiphoton microscope with a Zeiss 20 x objective (NA = 1). TdTomato fluorescence was excited at 980 nm using an InSight X3 tunable laser (Spectra-Physics) and collected through a 617/73 band-pass filter on a highly sensitive non-descanned detector. After the first imaging session, the mice woke up and were placed in a cage with their littermates for 4-5 h (P15-18). For the second imaging session the mice were again anesthetized with isoflurane (initially 3%, then 1-1.5% for anesthesia maintenance) and imaged to retrieve the same dendritic structures recorded in the first imaging session (see Supplementary Information).

Histology

Mice aged P30 were anesthetized with pentobarbital (150 mg/kg) and intracardially perfused with PBS followed by 4% buffered formaldehyde (Histofix, Roti). Free-floating sections were processed for immunohistochemistry as described in the Supplementary Information. Images were acquired using a confocal microscope (SP5, Leica) and analyzed according to procedures described in the Supplementary Information.

Acute slice preparation, *ex vivo* electrophysiology and optogenetics

250 µm-thick slices were prepared from brains of control and C4-OE mice. For patch-clamp recordings, slices were transferred to the recording chamber where they were continuously superfused with ACSF (30-32°C) buffered by continuous bubbling with 95% O_2-5% CO_2. Whole-cell current and voltage-clamp recordings were performed in PFC layer II/III. Stimulus delivery and data acquisition were performed using Patchmaster software (Multichannel Systems). Signals were acquired with an EPC10-usb amplifier (Multichannel Systems), sampled at 20 kHz and filtered at 4 kHz. For optogenetic experiments, pulses of blue light (wavelength 470 nm) were emitted by a light emitting diode (CoolLED). Offline analysis was performed using Clampfit (Molecular Devices) and Igor Pro (Wavemetrics). For the study of miniature post synaptic currents, recordings were filtered offline at 2 kHz and analyzed using MiniAnalysis (Synaptosoft). See Supplementary Information.

Behavior

Tests for locomotor activity (actimeter, Open Field), and working memory (learning of a Non-Matching-To-Sample task, Odor Span Test, Spatial Span Test) were performed and analyzed as described in the Supplementary Information.

Statistical analysis

Data are presented as mean ± SEM. Statistical analyses were performed using Prism (Graphpad). The normality of data distribution was tested using Shapiro-Wilk's test. Unpaired two-tailed T-tests (for normally distributed datasets) or Mann–Whitney tests (for non-normally distributed datasets) were used for comparisons between two groups. For multiple comparisons we used two-way ANOVA followed by Sidak's test. Values of $P < 0.05$ were considered statistically significant. P values are reported as follows: * $P < 0.05$; ** $P < 0.01$; *** $P < 0.001$; **** $P < 0.0001$.

Results

Generation of C4-overexpressing (C4-OE) mice using *in utero* electroporation

Using in utero electroporation in C57Bl/6J mice we selectively overexpressed the C4-encoding *C4b gene*, the mouse homolog of the human *C4A* and *C4B* genes, in layer II/III pyramidal cells of the prefrontal cortex (PFC). Targeted PFC areas included the cingulate, prelimbic and infralimbic cortices (Supplementary figure S1A). To identify C4-OE neurons using immunohistochemistry, an HA tag was added at the N-terminal end of the *C4b* overexpression construct before the signal peptide. In addition, we co-electroporated the *C4b* construct with a tdTomato-expressing construct, in order to enable the identification of C4-expressing, tdTomato-positive (tdTom+) neurons in acute brain slices (Supplementary figure S1B-C). To ensure that most tdTom+ neurons indeed overexpress C4, we co-electroporated the *C4b* construct and the tdTomato construct with a 4:1 ratio. Immunohistochemistry for HA and tdTomato confirmed that 98.7 ± 1.8 % of tdTom+ neurons also expressed C4 (Supplementary figure S1D-E). Control mice were electroporated with the tdTomato construct only. Due to the selectivity of the in utero electroporation procedure, which exclusively targets dividing progenitors of the ventricular zone, C4 overexpression was restricted to pyramidal cells. Interneurons or glial cells did not express the electroporated plasmids. Accordingly, all tdTomato-expressing cells had the characteristic morphology of cortical pyramidal cells, including a prominent apical dendrite projecting towards the pial surface. In immunoblots on lysates from the electroporated area, the HA tag was only detected at the molecular weight of the full-length form of C4 before its proteolytic cleavage (prepro-C4, ~ 200 kDa) in the C4-OE condition, suggesting that the HA tag was correctly cleaved together with the signal peptide (Supplementary figure S1F-G). To quantify C4 overexpression in the electroporated area using western blot, we first evaluated several anti-C4 antibodies and found that an anti-C4 antibody raised against a motif of the α-chain of human C4 reliably detected a band of the expected molecular weight in cortical tissue from control and C4-OE mice (Supplementary figure S1G). Using this antibody we found that C4 protein expression was increased approximately 1.38-fold in P30 mice in the C4-OE condition (Supplementary figure S1H). We observed no neuronal mispositioning in C4-OE mice, suggesting the absence of major migration defects (Supplementary figure S2).

Loss of excitatory synapses in C4-OE neurons from juvenile and adult, but not neonatal mice

We first evaluated passive and active cellular properties in tdTom+ layer II/III pyramidal cells using whole-cell patch-clamp *ex vivo*. The firing properties, membrane resistance, cell capacitance and resting membrane potential were similar in control and C4-OE neurons (Supplementary figure S3; Supplementary table S1). We next examined excitatory synaptic transmission at three developmental stages. The frequency of miniature excitatory postsynaptic currents (mEPSCs) in control tdTom+ cells markedly increased from early postnatal development (age P9-P10) to the juvenile stage (P25-P30), consistent with increased synapse generation, before decreasing from the juvenile stage to adulthood (P150-P220), in line with synapse elimination in the maturing cortex (Figure 1A-B; Supplementary table S1). The paired-pulse ratio of evoked EPSCs, a measure which is sensitive to alterations in presynaptic release probability, did not change significantly in control tdTom+ cells throughout development (Figure 1C-D; Supplementary table S1). Interestingly, mEPSC frequency was similar in control and C4-OE mice at P9-P10, but was significantly lower in C4-OE mice in juvenile and adult mice (Figure 1B; two-way ANOVA, $P < 0.0001$; juvenile: Sidak's post-hoc test $P < 0.0001$; adulthood: Sidak's post-hoc test, $P < 0.05$; Supplementary table S1). The paired-pulse ratio of evoked EPSCs did not differ between C4-OE and control mice in any age group (Figure 1D). We also observed a decrease in mEPSC amplitude from early development to the juvenile stage, but this was comparable in control and C4-OE mice (Figure 1B; Supplementary table S1).

C4 overexpression results in diminished formation and elimination of spines in juvenile PFC

To establish whether decreased functional excitatory input in C4-OE pyramidal cells correlates with reduced spine density, we imaged dendritic spines of tdTom+ pyramidal cells in layer I/II of the prefrontal cortex using *in vivo* 2-photon imaging in juvenile (P30) mice (Figure 1E). We found a substantial spine density decrease in C4-OE neurons (Figure 1F-G; T-test, $P = 0.0023$; Supplementary table S2). These results suggested that the reduction in spine density in C4-OE neurons is due to imbalanced spine dynamics (gain and loss) occurring prior to P30. Therefore, we performed dynamic imaging studies in mice aged P15-P18, which corresponds to a period of heightened structural synaptic plasticity[15-17]. Here, we imaged dendrites twice at a 4-hour interval (Figure 2A) to study fast spine kinetics at this stage of active synaptic reorganization. Similar to the P30 cohort, C4-OE neurons in P15-P18 mice displayed a robust decrease in spine density (Figure 2B-C; Mann Whitney Test, $P <$

0.0001; Supplementary table S2). While the overall spine density within the experimental groups did not change over the course of 4 h (Figure 2D-E; table S2), C4 overexpression had a strong effect on the structural plasticity of single spines; first, C4-OE neurons formed fewer stable spines (Figure 2F; T-test, $P = 0.0007$; Supplementary table S2). Second, C4-OE neurons showed decreased numbers of both gained and lost spines (Figure 2G-H; gained: T-test, $P = 0.0018$; lost: T-test, $P < 0.0001$; also see Figure 2F; Supplementary table S2) resulting in an overall significantly reduced turnover of dendritic spines (Figure 2I; T-test, $P = 0.0039$; Supplementary table S2). In summary we show here that C4 overexpression results in diminished formation/stabilization and elimination of spines in juvenile PFC *in vivo*. To study dendritic spines with improved spatial resolution, we imaged fixed post-mortem samples from P15-P18 control and C4-OE mice using confocal microscopy with an Airyscan detector, and obtained morphological reconstructions of dendritic spines using the Imaris software. These data confirmed the significant decrease in spine density in C4-OE neurons (Supplementary figure S4A-B; T-test, $P = 0.023$). We plotted key morphological parameters (dendritic spine length, maximum head diameter, ratio of mean head to neck diameters) in three dimensions. The 3D plot revealed differences in the distributions of the morphological parameters (Supplementary figure S4C). A cluster analysis[18] ('Agglomerative Hierarchical Clustering' analysis based on Euclidian distance in the parameter space, see Supplementary Materials and methods) revealed at least three distinct populations of spines, which resemble the different categories commonly used in the literature to classify dendritic spines ('small' ≅ cluster 1, 'thin' ≅ cluster 2 and 'mushroom-like' ≅ cluster 3; Supplementary figure S4D-F). The distribution of spines in the three clusters was similar in the control and C4-OE conditions (Supplementary figure S4E-F).

NMDAR hypofunction in C4-OE pyramidal cells

To investigate NMDAR-mediated transmission in the cortex of C4-OE mice, we measured the AMPA/NMDA ratio of evoked EPSCs in tdTom+ cells. The AMPA/NMDA ratio was comparable in control and C4-OE neonates, but was significantly increased in juvenile and adult C4-OE mice (Figure 3A-B; Two-way ANOVA, $P < 0.0001$; juvenile and adult mice: Sidak's test, $P < 0.001$; Supplementary table S1). The amplitude of mEPSCs, which is determined by the number of AMPAR per synapse, was not altered by C4 overexpression at any age examined (Figure 1B; Supplementary table S1). Furthermore, the decay time constant of NMDAR-mediated currents, which depends on the subunit composition of NMDA receptors, was similar in control and C4-OE mice of the same age group (Figure 3C;

Supplementary table S1). Therefore the increased AMPA/NMDA ratio in C4-OE neurons results from reduced NMDAR-mediated currents. Increased AMPA/NMDA ratio has been repeatedly associated with altered synaptic expression of the AMPAR GluA2 subunit[19, 20] that controls the calcium permeability of AMPARs[21, 22]. Therefore we assessed the rectification of synaptic AMPAR-mediated currents which is sensitive to the presence of the GluA2 subunit. We found that the rectification index of evoked AMPAR currents was significantly decreased in juvenile and adult C4-OE mice, but not in pups (Figure 3D-E; two-way ANOVA, $P < 0.0001$; juvenile: Sidak's test, $P < 0.001$; adulthood: Sidak's test, $P < 0.05$; Supplementary table S1). This suggests that synaptic AMPARs in C4-OE neurons show reduced GluA2 subunit content, thus becoming more calcium-permeable, concomitantly with NMDAR hypofunction.

C4 overexpression results in reduced GABAergic transmission

Abnormalities in GABAergic networks constitute another hallmark of the schizophrenic cortex. They include synaptic abnormalities as well as decreased expression of GAD67 in parvalbumin-expressing (PV) interneurons. We examined spontaneous inhibitory synaptic transmission in tdTom+ pyramidal cells from juvenile mice using a high chloride intracellular solution to maximize the signal/noise ratio. Both the frequency and amplitude of miniature inhibitory postsynaptic currents (mIPSCs) were significantly decreased in C4-OE neurons (Figure 4A-B; frequency: Mann-Whitney test, $P = 0.0004$; amplitude: T-test, $P = 0.0003$; Supplementary table S1). Reduced mIPSC frequency may result from decreased release probability from GABAergic terminals in the maternal immune activation (MIA) model of SZ[23] which has been associated with increased expression of complement C1q and C4[24, 25]. We investigated GABA release probability using a similar protocol[23]. IPSCs were evoked by four consecutive electrical stimuli delivered at 20 Hz while holding voltage-clamped tdTom+ pyramidal cells at a membrane potential of +10 mV (Figure 4C). Short-term synaptic depression, which is sensitive to changes in release probability, showed a non-significant trend towards reduction in C4-OE neurons (Figure 4D; RM two-way ANOVA, $P = 0.089$; Supplementary table S1). In the MIA model, altered release probability from PV neurons, but not from other types of interneurons, has been inferred from optogenetic studies of short-term plasticity[23]. We reasoned that selectively activating the PV neuron-pyramidal cells synapse in C4-OE mice might allow to uncover significant differences in short-term depression. To test this hypothesis, we expressed Channelrhodopsin2 (ChR2) fused to YFP in PV-expressing interneurons using timed matings between lox-STOP-lox ChR2 mice and PV-Cre mice

(Supplementary figure S5A). Pregnant females were electroporated at embryonic stage E15 either with a tdTomato-encoding plasmid (control group) or with tdTomato + C4 (C4-OE condition). To verify the specificity of ChR2 expression, we patched-clamped ChR2-YFP+ cells in the control group and recorded their firing pattern in response to a 500 ms pulse of blue light (470 nm). All tested ChR2-YFP cells exhibited the characteristic fast-spiking firing pattern of PV interneurons (n = 3 cells; Supplementary figure S5B). Light-evoked PSCs in pyramidal cells were blocked by GABAzine, confirming their GABAergic nature (Supplementary figure S5C-D). Next we assessed short-term depression of PV neuron IPSCs in pyramidal cells using four consecutive blue light pulses (0.5 ms) delivered at 20 Hz (Figure 4E). We found that PV neuron-pyramidal cell synapses in C4-OE mice displayed significantly reduced short-term depression, consistent with decreased GABA release probability (Figure 4F; RM two-way ANOVA, main effect, $P = 0.014$; Supplementary table S1). Thus, similar to the MIA model, decreased release probability from PV neurons may contribute to diminish GABAergic transmission onto pyramidal cells in C4-OE mice.

C4 overexpression in pyramidal cells causes reduced input resistance, decreased excitability, and lower GAD67 expression in PV neurons

The availability of presynaptic GABA is one of the factors determining release probability. GAD67 is an enzyme responsible for basal cortical GABA synthesis[26], and reduced expression of GAD67, especially in PV cells, has been found in post-mortem cortical tissue from schizophrenic patients in multiple studies[14, 27]. In mouse models, reducing GAD67 expression in PV neurons decreases both the frequency of spontaneous inhibitory currents[28] and the amplitude of evoked GABAergic currents in pyramidal cells[29]. Therefore we measured GAD67 expression in PV interneurons located in the vicinity of control or C4-OE tdTom+ pyramidal cells. As GAD67 is expressed in both presynaptic terminals and in the cell soma, we quantified GAD67 expression in the clearly delineated cell soma (Figure 4G)[23]. GAD67 expression in PV cells was significantly lower in C4-OE mice than in control mice (Mean intensity compared to control, T-test, $P = 0.0094$; Figure 4H; Supplementary table S2). These results suggest that reduced GABA synthesis may contribute to the deficit in GABAergic transmission at PV neuron – pyramidal cell synapses in C4-OE mice. It has been proposed that reduced expression of activity-dependent biomarkers, including GAD67, in PV neurons, may result from decreased PV neuron activity in the schizophrenic cortex[14]. We investigated the number and distribution of PV neurons in the cortex of C4-OE juvenile mice and found that they were not altered (Supplementary figure S6; Supplementary table S2). We

then electroporated C4 + tdTomato or tdTomato alone in PV-Cre::RCE mice which express EGFP selectively in PV neurons. We patch-clamped EGFP+ PV neurons located in the vicinity of tdTom+ pyramidal cells, in control and C4-OE mice aged P25-P30 (Figure 4I). The intrinsic excitability of PV neurons, i.e. their propensity to fire action potentials when subjected to an input current in the presence of drugs blocking synaptic transmission, was significantly diminished in the C4-OE condition (Figure 4J; RM two-way ANOVA, main effect $P = 0.013$; Supplementary table S3). This was associated with lower input resistance of PV cells (Figure 4K; Mann-Whitney test, $P = 0.0024$; Supplementary table S3), in the absence of significant changes in cell capacitance or resting membrane potential (Supplementary figure S7A-B; Supplementary table S3).

C4 overexpression results in increased excitatory input on PV neurons

Since synaptic inputs also contribute to neuronal excitability, we recorded miniature excitatory and inhibitory inputs (mEPSCs and mIPSCs) in EGFP+ PV neurons. We observed a significant increase in mEPSC frequency, and a trend towards increased mEPSC amplitude, in the C4-OE condition (Supplementary figure S7C-D; frequency: Mann-Whitney test, $P = 0.018$; amplitude: Mann-Whitney test, $P = 0.069$; Supplementary table S3). The paired-pulse ratio of evoked EPSCs in PV neurons remained unchanged (Supplementary figure S7E-F; table S3). Neither the frequency nor the amplitude of mIPSCs was changed following C4 overexpression in pyramidal cells (Supplementary figure S7G-H; Supplementary table S3). Thus, in contrast to C4-OE pyramidal cells, PV neurons exhibit increased excitatory input in C4-OE mice.

Working memory deficits in C4-OE mice

Finally we investigated whether the changes that we observed at the cellular level may result in long-lasting behavioral alterations in C4-OE mice. In SZ, deficits in working memory are central to cognitive impairments and appear to result, at least in part, from abnormalities in PFC function[30, 31]. Therefore we asked whether increased C4 expression in the PFC alters working memory. Since classical working memory tests rely on locomotion, we first verified that control and C4-OE mice showed comparable spontaneous locomotor activity in an actimeter (Figure 5A; Supplementary table S4). Spontaneous activity of C4-OE mice also did not differ from control mice in the open field assay (Figure 5B; Supplementary table S4). We then used two different tests of working memory, namely the odor span test and the spatial span test. C4-OE mice performed equally well as control mice during the acquisition of the

non-matching to sample task, in which mice learned to associate the presence of a new odor and food reward (Figure 5C-E; Supplementary table S4). In the subsequent span tests, however, when mice had to remember an increasing number of odors or positions to obtain the reward, C4-OE mice exhibited reduced working memory capacity compared to control mice (Figure 5F-I; odor span: Mann-Whitney test, $P = 0.0022$; spatial span: Mann-Whitney test, $P = 0.045$; Supplementary table S4). Taken together, these results indicate that working memory is impaired in C4-OE mice, in line with neuronal abnormalities in PFC networks.

Discussion

GWAS have provided unprecedented identification of predisposing genetic risk factors in SZ. High expression variants of the C4 gene contribute to the strong association between SZ and a genomic region within the MHC locus on Chromosome 6 in GWAS[4, 5]. Here we show that overexpressing C4 in the mouse PFC recapitulates several cortical phenotypes associated with SZ, including synapse loss, decreased NMDAR-mediated neurotransmission, impaired function of GABAergic circuits, and deficits in working memory (Supplementary figure S8).

Decreased spine turnover in C4-OE mice

Elevated expression of C4 in neurons enhances microglia-mediated synaptic engulfment[10-12]. Our *in vivo* imaging results clearly show an overall decrease in gained and lost dendritic spines in juvenile mice as a consequence of C4 overexpression. This apparent discrepancy may reflect an underappreciated role of complement in regulating spine formation or immature spine stabilization. The decrease in spine turnover observed in our model could be due to excessive microglial phagocytosis of the synapses in formation or just formed, preventing their stabilization. The disappearance of these spines in less than 4 hours, the time window used for our time-lapse 2-photon microscopy acquisitions, would thus result in decreased spine gain.

Time course of synaptic deficits in C4-OE mice

It is noteworthy that the decrease in excitatory input to C4-OE neurons is not present at the early stages of postnatal development, but only appears between P10 and P25, a period of strong synaptic remodeling in the cortex. This may be relevant for the pathophysiology of SZ, a disorder in which even the earliest prodromal symptoms occur at a relatively late stage of postnatal development. The reduction in NMDAR-mediated transmission is concomitant with the loss of functional excitatory synapses in C4-OE mice, suggesting that C4 overexpression

may selectively impair the formation or maintenance of "weak" (high NMDAR, low AMPAR) synapses in juvenile mice. Another study reported that synaptic deficits were accompanied by a decrease in cellular capacitance in C4-OE pyramidal cells[11]. We found that cell capacitance was unchanged following C4-OE. While we cannot exclude that different experimental settings account for this difference, the absence of significant changes in capacitance may be in line with the unchanged morphology of C4-OE pyramidal neurons[11]. We show that synaptic deficits persist into adulthood in C4-OE mice. Our immunohistochemistry results indicate that C4 is still overexpressed in the PFC of adult C4-OE mice, suggesting that increased C4 expression may persistently affect spine turnover in C4-OE mice. However, since synaptic refinement is particularly pronounced in the developing cortex[16, 17], it is likely that elevated expression of C4 predominantly affects circuit remodeling in juvenile mice.

GABAergic network abnormalities

While another study did not detect significant changes in the inhibitory input to C4-OE pyramidal cells[11], we observed a significant reduction in mIPSC frequency and amplitude. This discrepancy may be due to the higher driving force for chloride ions at hyperpolarized membrane potentials, and hence improved signal/noise ratio of IPSC recordings, in our experimental conditions of high intracellular chloride. We also show that C4-OE in pyramidal cells decreases GABA release from PV neurons onto pyramidal cells, consistent with decreased GAD67 expression in PV neurons and reduced PV neuron excitability. The cause of the well-substantiated decrease in GAD67 cortical expression in SZ is unclear. It has been hypothesized that lower activity of layer II/III pyramidal cells, possibly due to their reduced number of dendritic spines, could result in fewer excitatory inputs onto PV cells (for instance through lower neuronal activity-regulated pentraxin secretion from pyramidal cells), leading to reduced PV neuron excitation and hence decreased activity-dependent GAD67 expression[14, 32]. In C4-OE mice, reduced GAD67 expression in PV neurons may result from altered intrinsic properties of PV neurons as a consequence of homeostatic adaptation to reduced network activity, rather than from decreased synaptic excitatory input. Indeed we show that PV neuron excitability is impaired in C4-OE mice, while increased mEPSC frequency in PV neurons indicates that PV neurons are spared from excitatory synapse loss associated with C4 overexpression in pyramidal cells.

Linking neural dysfunctions and cognitive impairment in C4-OE mice

Cognitive dysfunction is a central feature of SZ that is not treated by current pharmacotherapy, and determines the functional outcome of the illness[33]. Impaired working memory has been proposed to be central in the cognitive impairments associated with SZ[30, 31]. Spine loss, reduced NMDAR transmission and PV neuron dysfunction in the PFC may all contribute to impair working memory. For example, decreased cortical connectivity in SZ has repeatedly been associated with working memory deficits[34]. Decreased synapse density in layer II/III may particularly affect connectivity, since layer II/III pyramidal cells make major contributions to cortico-cortical connections, including callosal connections, and therefore integrate information across cortical areas and hemispheres. Furthermore, blocking NMDA, but not AMPA, receptors during a working memory task abolishes persistent activity in prefrontal neurons[35]. Finally, PV neurons contribute to the mechanisms underlying working memory[36], in line with the well-established role of PV neurons in the generation of fast, gamma frequency oscillations in neocortex[37, 38]. Our results suggest that these distinct alterations occur together during development as a consequence of elevated C4 expression, making it difficult to attribute cognitive dysfunction to a single one of them. The combination of reduced connectivity, NMDAR hypofunction and altered PV neuron function might collectively modify the dynamics of specific attractors, which are thought to be the substrate for persistent neural activity underlying short-term memory[39, 40].

Conclusion

Decreased spine density, reduced NMDAR function, and alterations in GABAergic networks have been associated with SZ. We show that elevated C4 expression in PFC pyramidal cells results in functional alterations that are consistent with these SZ-associated phenotypes, and causes working memory impairment, a characteristic feature of cognitive deficits in SZ. In particular, we propose that the persistent decrease in NMDAR-mediated neurotransmission in C4-OE mice might be the consequence of impaired stabilization of immature synapses. This could provide a conceptual framework to relate the hypotheses of excessive synaptic pruning and NMDAR hypofunction in SZ.

Conflict of interest

The authors declare no conflict of interest.

Acknowledgements

MD was the recipient of fellowships from Sorbonne University and from FRM/Venite Cantemus (FDT20190400802). The project was supported by funds from the Investissements d'Avenir program under reference ANR-11-IDEX-0004-02 to CLM and RT, the Emergence program of Sorbonne University to CLM, and from an ERANET Neuron Grant to RT (ANR-18-0008-01), MF (BMBF 01EW1905) and CLM (ANR-18-0008-02). We thank Drs L Maroteaux, P Gaspar and J-C Poncer for critically reading the manuscript.

References

1. Purcell SM, Wray NR, Stone JL, Visscher PM, O'Donovan MC, Sullivan PF *et al.* Common polygenic variation contributes to risk of schizophrenia and bipolar disorder. *Nature* 2009; **460**(7256)**:** 748-752.

2. Shi J, Levinson DF, Duan J, Sanders AR, Zheng Y, Pe'er I *et al.* Common variants on chromosome 6p22.1 are associated with schizophrenia. *Nature* 2009; **460**(7256)**:** 753-757.

3. Stefansson H, Ophoff RA, Steinberg S, Andreassen OA, Cichon S, Rujescu D *et al.* Common variants conferring risk of schizophrenia. *Nature* 2009; **460**(7256)**:** 744-747.

4. Ripke S, Neale BM, Corvin A, al. e. Biological insights from 108 schizophrenia-associated genetic loci. *Nature* 2014; **511**(7510)**:** 421-427.

5. Sekar A, Bialas AR, de Rivera H, Davis A, Hammond TR, Kamitaki N *et al.* Schizophrenia risk from complex variation of complement component 4. *Nature* 2016; **530**(7589)**:** 177-183.

6. Stevens B, Allen NJ, Vazquez LE, Howell GR, Christopherson KS, Nouri N *et al.* The classical complement cascade mediates CNS synapse elimination. *Cell* 2007; **131**(6)**:** 1164-1178.

7. Glantz LA, Lewis DA. Decreased dendritic spine density on prefrontal cortical pyramidal neurons in schizophrenia. *Arch Gen Psychiatry* 2000; **57**(1)**:** 65-73.

8. Feinberg I. Schizophrenia: caused by a fault in programmed synaptic elimination during adolescence? *Journal of psychiatric research* 1982; **17**(4)**:** 319-334.

9. Prasad KM, Chowdari KV, D'Aiuto LA, Iyengar S, Stanley JA, Nimgaonkar VL. Neuropil contraction in relation to Complement C4 gene copy numbers in independent cohorts of adolescent-onset and young adult-onset schizophrenia patients-a pilot study. *Translational psychiatry* 2018; **8**(1)**:** 134.

10. Sellgren CM, Gracias J, Watmuff B, Biag JD, Thanos JM, Whittredge PB *et al.* Increased synapse elimination by microglia in schizophrenia patient-derived models of synaptic pruning. *Nat Neurosci* 2019; **22**(3)**:** 374-385.

11. Comer AL, Jinadasa T, Sriram B, Phadke RA, Kretsge LN, Nguyen TPH *et al.* Increased expression of schizophrenia-associated gene C4 leads to hypoconnectivity of prefrontal cortex and reduced social interaction. *PLoS Biol* 2020; **18**(1)**:** e3000604.

12. Yilmaz M, Yalcin E, Presumey J, Aw E, Ma M, Whelan CW *et al.* Overexpression of schizophrenia susceptibility factor human complement C4A promotes excessive synaptic loss and behavioral changes in mice. *Nat Neurosci* 2020.

13. Balu DT. The NMDA Receptor and Schizophrenia: From Pathophysiology to Treatment. *Adv Pharmacol* 2016; **76:** 351-382.

14. Dienel SJ, Lewis DA. Alterations in cortical interneurons and cognitive function in schizophrenia. *Neurobiol Dis* 2019; **131:** 104208.

15. Coiro P, Padmashri R, Suresh A, Spartz E, Pendyala G, Chou S *et al.* Impaired synaptic development in a maternal immune activation mouse model of neurodevelopmental disorders. *Brain Behav Immun* 2015; **50:** 249-258.

16. Zuo Y, Lin A, Chang P, Gan WB. Development of long-term dendritic spine stability in diverse regions of cerebral cortex. *Neuron* 2005; **46**(2)**:** 181-189.

17. Holtmaat AJ, Trachtenberg JT, Wilbrecht L, Shepherd GM, Zhang X, Knott GW *et al.* Transient and persistent dendritic spines in the neocortex in vivo. *Neuron* 2005; **45**(2)**:** 279-291.

18. Pfeiffer T, Poll S, Bancelin S, Angibaud J, Inavalli VK, Keppler K *et al.* Chronic 2P-STED imaging reveals high turnover of dendritic spines in the hippocampus in vivo. *eLife* 2018; **7**.

19. Bellone C, Luscher C. Cocaine triggered AMPA receptor redistribution is reversed in vivo by mGluR-dependent long-term depression. *Nat Neurosci* 2006; **9**(5)**:** 636-641.

20. Wang HX, Gao WJ. Development of calcium-permeable AMPA receptors and their correlation with NMDA receptors in fast-spiking interneurons of rat prefrontal cortex. *J Physiol* 2010; **588**(Pt 15)**:** 2823-2838.

21. Hollmann M, Hartley M, Heinemann S. Ca2+ permeability of KA-AMPA--gated glutamate receptor channels depends on subunit composition. *Science* 1991; **252**(5007)**:** 851-853.

22. Geiger JR, Melcher T, Koh DS, Sakmann B, Seeburg PH, Jonas P *et al.* Relative abundance of subunit mRNAs determines gating and Ca2+ permeability of AMPA receptors in principal neurons and interneurons in rat CNS. *Neuron* 1995; **15**(1)**:** 193-204.

23. Canetta S, Bolkan S, Padilla-Coreano N, Song LJ, Sahn R, Harrison NL *et al.* Maternal immune activation leads to selective functional deficits in offspring parvalbumin interneurons. *Mol Psychiatry* 2016; **21**(7)**:** 956-968.

24. Duchatel RJ, Meehan CL, Harms LR, Michie PT, Bigland MJ, Smith DW *et al.* Increased complement component 4 (C4) gene expression in the cingulate cortex of rats exposed to late gestation immune activation. *Schizophr Res* 2018; **199:** 442-444.

25. Han M, Zhang JC, Hashimoto K. Increased Levels of C1q in the Prefrontal Cortex of Adult Offspring after Maternal Immune Activation: Prevention by 7,8-Dihydroxyflavone. *Clinical*

psychopharmacology and neuroscience : the official scientific journal of the Korean College of Neuropsychopharmacology 2017; **15**(1)**:** 64-67.

26. Asada H, Kawamura Y, Maruyama K, Kume H, Ding RG, Kanbara N *et al.* Cleft palate and decreased brain gamma-aminobutyric acid in mice lacking the 67-kDa isoform of glutamic acid decarboxylase. *Proc Natl Acad Sci U S A* 1997; **94**(12)**:** 6496-6499.

27. Hashimoto T, Volk DW, Eggan SM, Mirnics K, Pierri JN, Sun Z *et al.* Gene expression deficits in a subclass of GABA neurons in the prefrontal cortex of subjects with schizophrenia. *J Neurosci* 2003; **23**(15)**:** 6315-6326.

28. Brown JA, Ramikie TS, Schmidt MJ, Baldi R, Garbett K, Everheart MG *et al.* Inhibition of parvalbumin-expressing interneurons results in complex behavioral changes. *Mol Psychiatry* 2015; **20**(12)**:** 1499-1507.

29. Fujihara K, Miwa H, Kakizaki T, Kaneko R, Mikuni M, Tanahira C *et al.* Glutamate Decarboxylase 67 Deficiency in a Subset of GABAergic Neurons Induces Schizophrenia-Related Phenotypes. *Neuropsychopharmacology* 2015; **40**(10)**:** 2475-2486.

30. Silver H, Feldman P, Bilker W, Gur RC. Working memory deficit as a core neuropsychological dysfunction in schizophrenia. *Am J Psychiatry* 2003; **160**(10)**:** 1809-1816.

31. Silver H, Feldman P. Evidence for sustained attention and working memory in schizophrenia sharing a common mechanism. *The Journal of neuropsychiatry and clinical neurosciences* 2005; **17**(3)**:** 391-398.

32. Hoftman GD, Datta D, Lewis DA. Layer 3 Excitatory and Inhibitory Circuitry in the Prefrontal Cortex: Developmental Trajectories and Alterations in Schizophrenia. *Biol Psychiatry* 2017; **81**(10)**:** 862-873.

33. Kahn RS, Keefe RS. Schizophrenia is a cognitive illness: time for a change in focus. *JAMA psychiatry* 2013; **70**(10)**:** 1107-1112.

34. Cao H, Dixson L, Meyer-Lindenberg A, Tost H. Functional connectivity measures as schizophrenia intermediate phenotypes: advances, limitations, and future directions. *Curr Opin Neurobiol* 2016; **36:** 7-14.

35. Wang M, Yang Y, Wang CJ, Gamo NJ, Jin LE, Mazer JA *et al.* NMDA receptors subserve persistent neuronal firing during working memory in dorsolateral prefrontal cortex. *Neuron* 2013; **77**(4)**:** 736-749.

36. Rossi MA, Hayrapetyan VY, Maimon B, Mak K, Je HS, Yin HH. Prefrontal cortical mechanisms underlying delayed alternation in mice. *J Neurophysiol* 2012; **108**(4)**:** 1211-1222.

37. Cardin JA, Carlen M, Meletis K, Knoblich U, Zhang F, Deisseroth K *et al.* Driving fast-spiking cells induces gamma rhythm and controls sensory responses. *Nature* 2009; **459**(7247)**:** 663-667.

38. Uhlhaas PJ, Singer W. Abnormal neural oscillations and synchrony in schizophrenia. *Nat Rev Neurosci* 2010; **11**(2)**:** 100-113.

39. Brody CD, Romo R, Kepecs A. Basic mechanisms for graded persistent activity: discrete attractors, continuous attractors, and dynamic representations. *Curr Opin Neurobiol* 2003; **13**(2)**:** 204-211.

40. Inagaki HK, Fontolan L, Romani S, Svoboda K. Discrete attractor dynamics underlies persistent activity in the frontal cortex. *Nature* 2019; **566**(7743)**:** 212-217.

Figure legends

Figure 1. Reduced excitatory input onto C4-OE pyramidal cells

(A) Sample traces of mEPSCs in control and C4-OE pyramidal cells at three developmental stages; scale bars: 20pA/100ms.

(B) mEPSC frequency was affected by C4-OE in juvenile and adult mice, but not in pups (two-way ANOVA, main effect, **** $P < 0.0001$; Sidak's post-hoc test #### $P < 0.0001$, # $P < 0.05$, n.s. not significant). mEPSC amplitude was not significantly affected (control: early postnatal, n = 21 cells from 3 mice; juvenile, n = 16 cells from 5 mice; adult, n = 20 cells from 4 mice; C4-OE: early postnatal, n = 21 cells from 3 mice; juvenile, n = 16 cells from 5 mice; adult, n = 20 cells from 4 mice).

(C) Average traces of eEPSCs evoked by paired-pulse stimulation with 50 ms interpulse interval, recorded from control and C4-OE pyramidal cells at three developmental stages; scale bars: 50 pA/50 ms.

(D) Similar paired-pulse ratio in control and C4-OE pyramidal cells (n.s., not significant. control: early postnatal, n = 16 cells from 3 mice; juvenile, n = 17 cells from 3 mice; adult, n = 19 cells from 5 mice; C4-OE: early postnatal, n = 21 cells from 3 mice; juvenile, n = 21 cells from 3 mice; adult, n = 17 cells from 4 mice). All data are represented as mean ± SEM. Each open circle represents an individual cell.

(E) Left, schematic drawing illustrating two-photon *in vivo* imaging in PFC at P30. Right, cranial window.

(F) Examples of apical dendrites from electroporated pyramidal cells in control and C4-OE mice aged P30.

(G) C4-OE decreased dendritic spine density in electroporated pyramidal cells from P30 mice; scale bar: 2 μm. (T-test, ** $P < 0.023$; control: n = 10 mice; C4-OE: n = 7 mice). All data are represented as mean ± SEM. Each open circle represents an individual mouse.

Figure 2. Decreased spine turnover in young (P15-P18) C4-OE mice

(A) Experimental timeline of *in vivo* two-photon imaging to investigate spine formation and elimination in electroporated pyramidal neurons. Spines already present at t_0 are in blue; spines that were stable, gained or lost at t_0 + 4h are in blue, green and magenta, respectively.

(B) Examples of apical dendrites from control and C4-OE electroporated pyramidal neurons imaged at t_0; scale bar: 2 μm.

(C) Spine density at t_0 in tdTom+ pyramidal neurons (t-test, **** $P < 0.0001$; control: n = 5 mice; C4-OE: n = 7 mice).

(D) Example images showing spine turnover from t_0 to t_0 + 4h in control and C4-OE pyramidal cells; scale bar: 2 μm.

(E) Evolution of the spine density between t_0 and t_0 + 4h in control and control and C4-OE pyramidal cells (control: n = 5 mice; C4-OE: n = 7 mice).

(F-H) Stable, gained and lost spine density in control and C4-OE neurons. C4-OE caused a significant reduction in the number of both gained and lost spines (stable spine: T-test, *** $P = 0.0007$; gained spines: t-test, ** $P = 0.0018$; lost spines: T-test, **** $P < 0.0001$; control: n = 5 mice; C4-OE: n = 7 mice).

(I) Spine turnover in control and C4-OE dendrites. The turnover rate is decreased in C4-OE dendrites (Mann-Whitney test, ** $P = 0.0039$; control: n = 5 mice; C4-OE: n = 7 mice).

All data are represented as mean ± SEM. Each open circle represents an individual mouse.

Figure 3. Altered AMPA/NMDA ratio and AMPAR rectification index in C4-OE mice

(A) Sample traces of evoked synaptic AMPA and NMDA currents recorded at -65 mV and +55 mV respectively in the presence of GABAzine at 3 developmental stages; The NMDAR component was measured 50 ms after stimulation (arrows). The AMPAR component was measured as the peak of the evoked EPSC at -65mV. Scale bars: 50pA/50ms.

(B-C) AMPA/NMDA ratio and NMDA decay time throughout development in control and C4-OE pyramidal cells. The AMPA/NMDA ratio was increased in C4-OE neurons from juvenile and adult mice, but not from neonates. The decay time of NMDARs was not affected by C4-OE at any stage of development, indicating that C4-OE does not alter NMDAR subunit

composition. This together with unchanged mEPSC amplitude in C4-OE mice (Fig.2B) indicates that the increased AMPA/NMDA ratio reflects reduced NMDAR-mediated excitatory transmission in C4-OE pyramidal neurons (two-way ANOVA, main effect, **** $P < 0.0001$, Sidak's post-hoc test ### $P < 0.001$; n.s., not significant. Control: early postnatal, n = 17 cells from 3 mice; juvenile, n = 23 cells from 4 mice; adult, n = 17 cells from 4 mice; C4-OE: early postnatal, n = 21 cells from 3 mice; juvenile, n = 20 cells from 5 mice; adult, n = 16 cells from 4 mice).

(D) Sample traces of evoked AMPA-mediated currents recorded at -65mV and +55mV at 3 developmental stages; scale bars: 50 pA/50 ms.

(E) The rectification index of AMPR-mediated currents was decreased in pyramidal cells from juvenile and adult C4-OE mice, suggesting the insertion of GluA2 subunit-lacking AMPAR at excitatory synapses (two-way ANOVA, **** $P < 0.0001$, Sidak's post-hoc test ## $P < 0.01$, # $P < 0.05$. Control: early postnatal, n = 20 cells from 3 mice; juvenile, n = 21 cells from 3 mice; adult, n = 17 cells from 4 mice; C4-OE: early postnatal, n = 20 cells from 3 mice; juvenile, n = 16 cells from 3 mice; adult, n = 24 cells from 3 mice). All data are represented as mean ± SEM. Each open circle represents an individual cell.

Figure 4. Alterations of GABAergic networks in C4-OE mice

(A) Sample traces of mIPSCs recordings at a holding potential of −65 mV in control and C4-OE pyramidal cells from juvenile mice (P25-P30); scale bars: 20pA/100ms.

(B) Both mIPSC frequency and amplitude were decreased in C4-OE pyramidal cells (frequency: Mann-Whitney test *** $P = 0.0004$; amplitude: t-Test *** $P = 0.0003$. Control: n = 16 cells from 4 mice; C4-OE: n = 16 cells from 4 mice).

(C) Schematic drawing illustrating the electrical stimulation of GABAergic release onto electroporated pyramidal cells (left) and example traces of 4 consecutive eIPSCs evoked with 50ms interpulse intervals, in control and C4-OE pyramidal cells (right); scale bars: 50 pA/50 ms.

(D) Ratios of the second, third and fourth eIPSC peak amplitude to the first eIPSC peak amplitude. Paired-pulse depression exhibited a trend towards being decreased in C4-OE neurons (two-way RM ANOVA, main effect, $P = 0.089$. Control: n = 29 cells from 3 mice; C4-OE: n = 37 cells from 3 mice).

(E) Schematic drawing illustrating the optogenetic activation of PV neuron and resulting IPSC recorded in electroporated pyramidal cells (left); and example traces of 4 consecutive light-evoked IPSCs with 50 ms interpulse intervals in control and C4-OE pyramidal cells (right); scale bars: 50 pA/50 ms.

(F) Ratios of the second, third and fourth light-evoked IPSC peak amplitude to the first IPSC peak amplitude. The increased ratio in C4-OE pyramidal cells indicates reduced presynaptic GABA release at PV neuron-pyramidal cell synapses (two-way RM ANOVA, main effect, * $P = 0.014$, Sidak's post-hoc test # $P < 0.05$. Control: n = 43 cells from 4 mice; C4-OE: n = 30 cells from 3 mice). All data are represented as mean ± SEM. Each open circle represents an individual cell.

(G) Example of immunostainings for tdTomato/PV and GAD67 on PFC slices from control and C4-OE mice. Arrows indicate GAD67-expressing PV cells; scale bar: 20µm.

(H) Mean intensity ± SEM of GAD67 expression in PV+ cells. GAD67 expression in PV cells was decreased in C4-OE mice (T-test; ** $P = 0.0094$; control: n = 28 mice; C4-OE: 33 mice). Each open circles represents an individual mouse.

(I) Schematic drawing depicting the patch-clamp recording of a PV interneuron located in the vicinity of tdTomato pyramidal cells (left) and sample spike trains in PV interneurons evoked by a 250 pA somatic current injection in control and C4-OE mice in the presence of synaptic blockers (right); scale bars: 20 mV/100 ms.

(J) PV interneurons exhibited reduced intrinsic excitability in C4-OE mice (two-way RM ANOVA, main effect, * $P = 0.013$. Control: n = 20 cells from 3 mice; C4-OE: n = 21 cells from 4 mice).

(K) The input resistance of PV neurons was significantly decreased in C4-OE mice (Mann-Whitney test, ** $P = 0.0024$. Control: n = 20 cells from 3 mice; C4-OE: n = 21 cells from 4 mice). Each open circle represents an individual cell.

Figure 5. Impaired working memory in C4-OE mice

(A) Locomotor activity measured at weaning in an actimeter, in control (n = 32 mice) and C4-OE male mice (n = 21 mice). Each dot represents spontaneous activity averaged over a period of 5 minutes.

(B) Locomotor activity measured one week after weaning in the open field, in control (n = 20 mice) and C4-OE mice (n = 14 mice).

(C) Time line of working memory tests. Animals were first trained to dig into scented sawdust to find a reward pellet (shaping) before learning a non-matching to sample (NMTS) task, followed by 4 days of odour span test, and 4 days of spatial span test.

(D) NMTS test procedure. Mice were exposed to pairs of odors and learned to associate a new odor with a reward.

(E) Performance in the NMTS odor test was similar in control and C4-OE mice (Control: n = 15 mice; C4-OE: 14 mice).

(F) Mice were exposed to an increasing number of odors in the odor span test.

(G) Working memory capacity in the odor span test is impaired in C4-OE mice (Control: n = 15 mice; C4-OE: 14 mice; Mann-Whitney test, ** $P = 0.0022$).

(H) Mice were exposed to an increasing number of positions in the spatial span test.

(I) Working memory capacity in the spatial span test is also affected in C4-OE mice (Control: n = 15 mice; C4-OE: 14 mice; Mann-Whitney test, * $P = 0.0448$).

All data are represented as mean ± SEM. Each open circle represents an individual mouse.

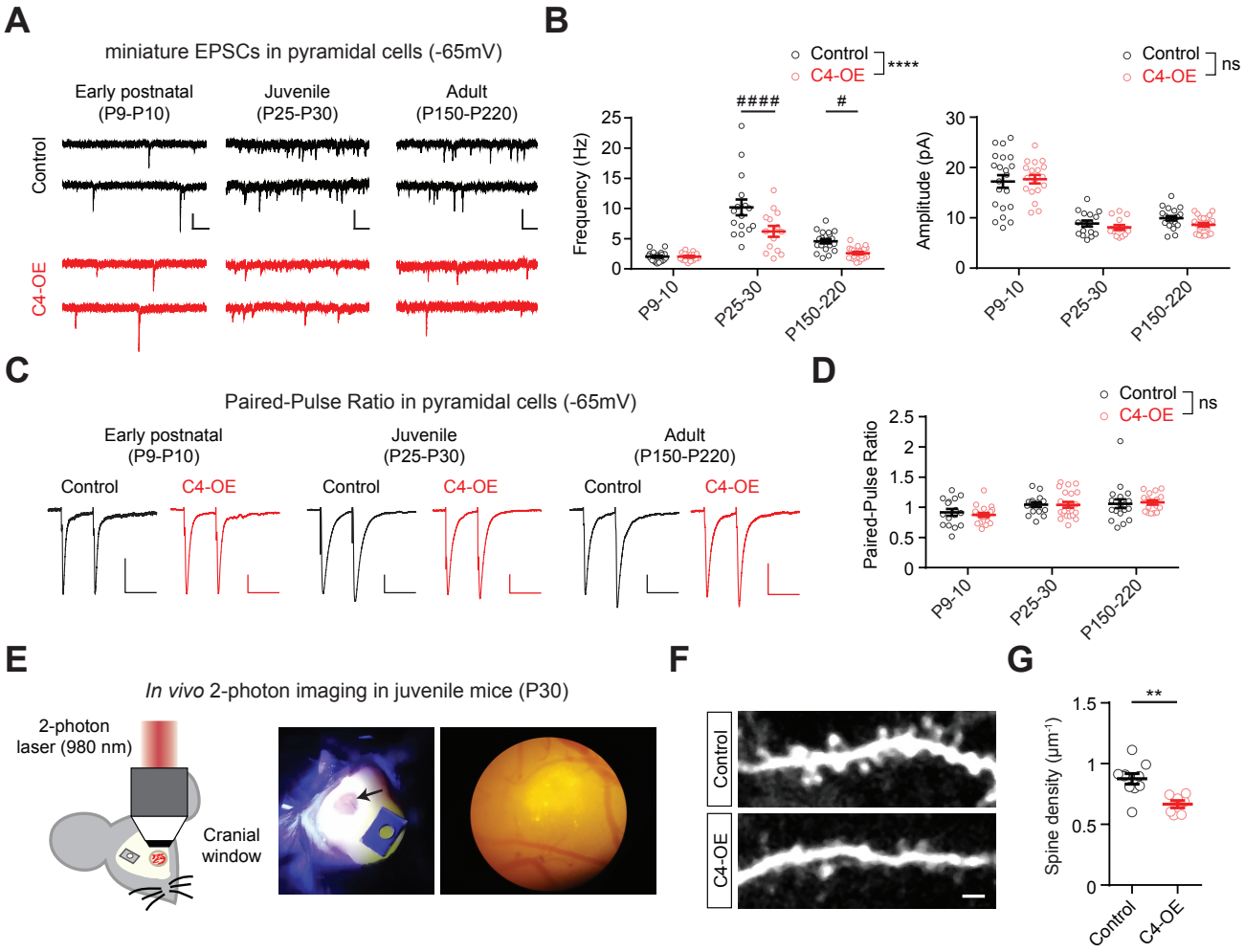
A
miniature EPSCs in pyramidal cells (-65mV)
Early postnatal (P9-P10)
Juvenile (P25-P30)
Adult (P150-P220)
Control
C4-OE
B
Control
C4-OE
****
ns
####
#
Frequency (Hz)
Amplitude (pA)
P9-10
P25-30
P150-220
C
Paired-Pulse Ratio in pyramidal cells (-65mV)
Early postnatal (P9-P10)
Juvenile (P25-P30)
Adult (P150-P220)
Control
C4-OE
D
Paired-Pulse Ratio
E
In vivo 2-photon imaging in juvenile mice (P30)
2-photon laser (980 nm)
Cranial window
F
G
Spine density (µm-1)
**

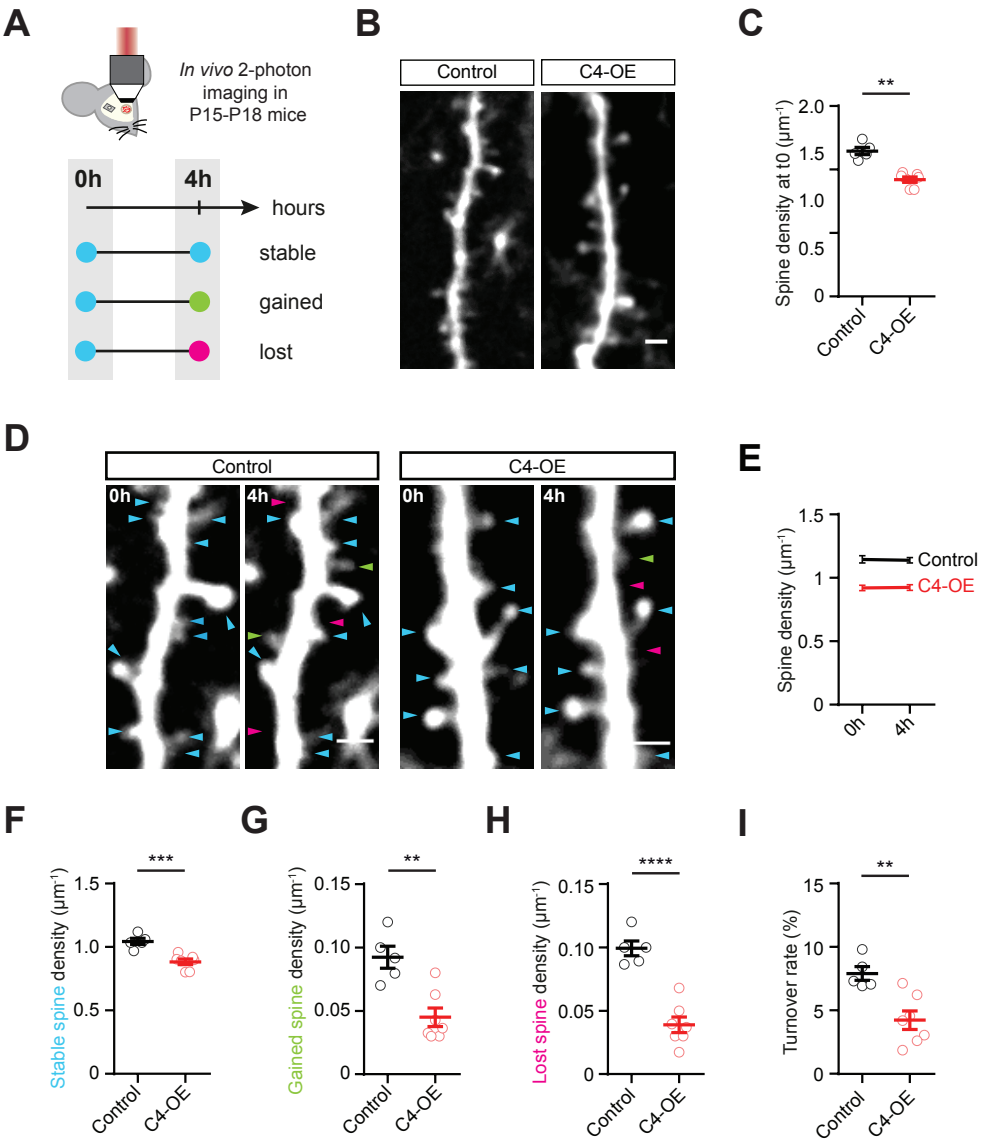
A
In vivo 2-photon imaging in P15-P18 mice
0h
4h
hours
stable
gained
lost
B
Control
C4-OE
C
Spine density at t0 (µm⁻¹)
2.0
1.5
1.0
0.5
0
**
Control
C4-OE
D
Control
C4-OE
0h
4h
0h
4h
E
Spine density (µm⁻¹)
1.5
1
0.5
0
Control
C4-OE
0h
4h
F
Stable spine density (µm⁻¹)
1.5
1.0
0.5
0
***
Control
C4-OE
G
Gained spine density (µm⁻¹)
0.15
0.10
0.05
0
**
Control
C4-OE
H
Lost spine density (µm⁻¹)
0.15
0.10
0.05
0
****
Control
C4-OE
I
Turnover rate (%)
15
10
5
0
**
Control
C4-OE

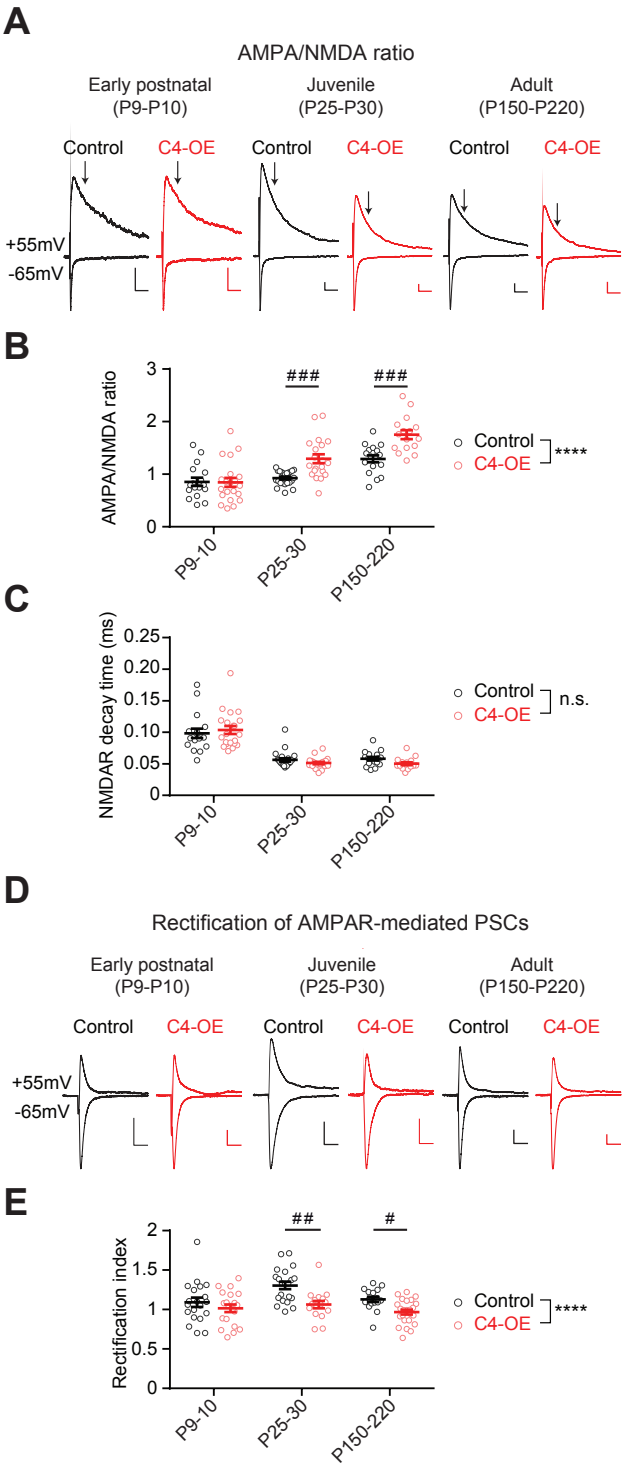
A
AMPA/NMDA ratio
Early postnatal (P9-P10)
Juvenile (P25-P30)
Adult (P150-P220)
Control
C4-OE
+55mV
-65mV
B
AMPA/NMDA ratio
###
Control
C4-OE
****
P9-10
P25-30
P150-220
C
NMDAR decay time (ms)
n.s.
D
Rectification of AMPAR-mediated PSCs
E
Rectification index
##
#

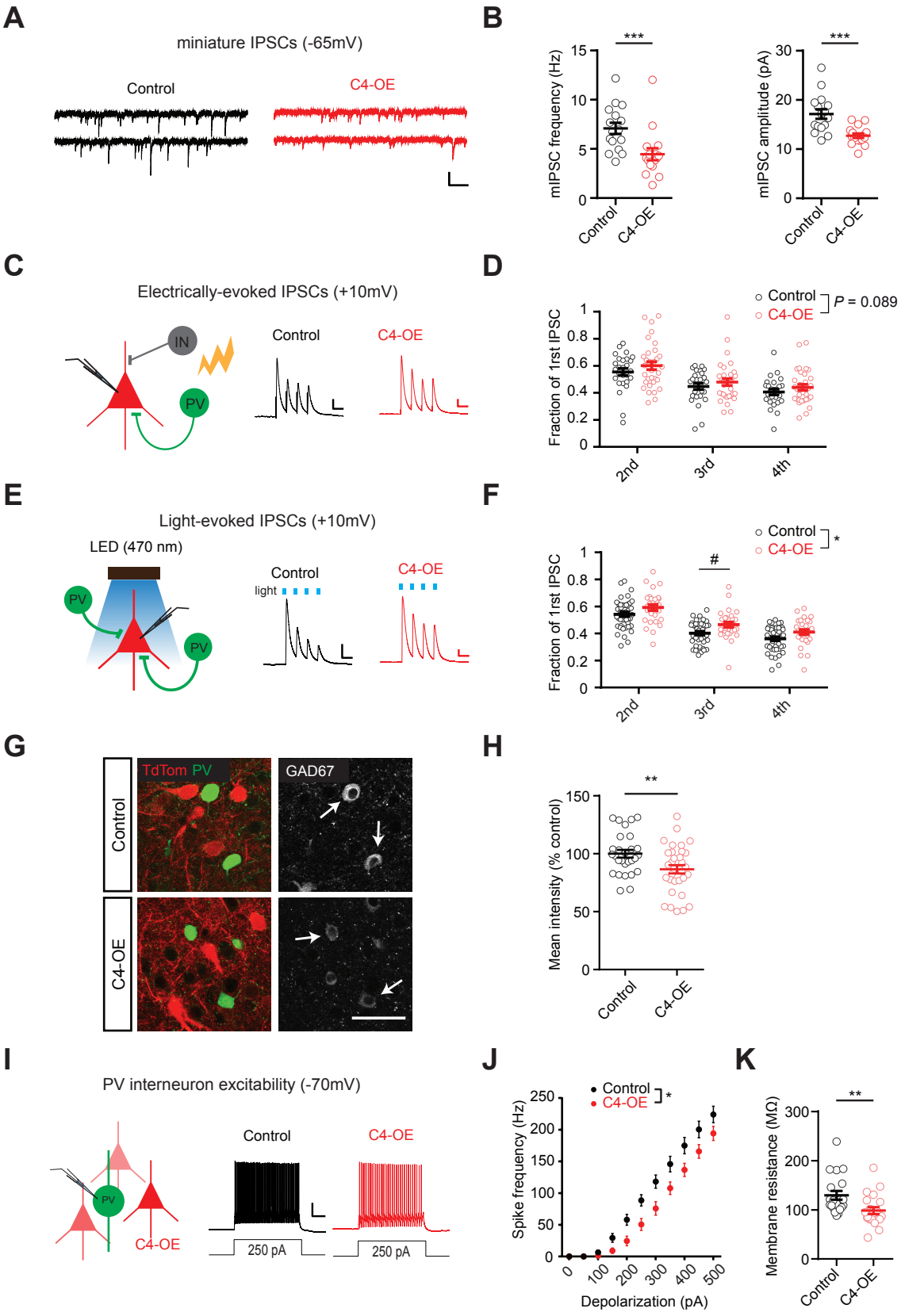
A
miniature IPSCs (-65mV)
Control
C4-OE
B
mIPSC frequency (Hz)
mIPSC amplitude (pA)
***
Control
C4-OE
C
Electrically-evoked IPSCs (+10mV)
IN
PV
Control
C4-OE
D
Fraction of 1rst IPSC
Control
C4-OE
P = 0.089
2nd
3rd
4th
E
Light-evoked IPSCs (+10mV)
LED (470 nm)
light
F
#
*
G
Control
C4-OE
TdTom PV
GAD67
H
Mean intensity (% control)
**
I
PV interneuron excitability (-70mV)
250 pA
J
Spike frequency (Hz)
Depolarization (pA)
K
Membrane resistance (MΩ)

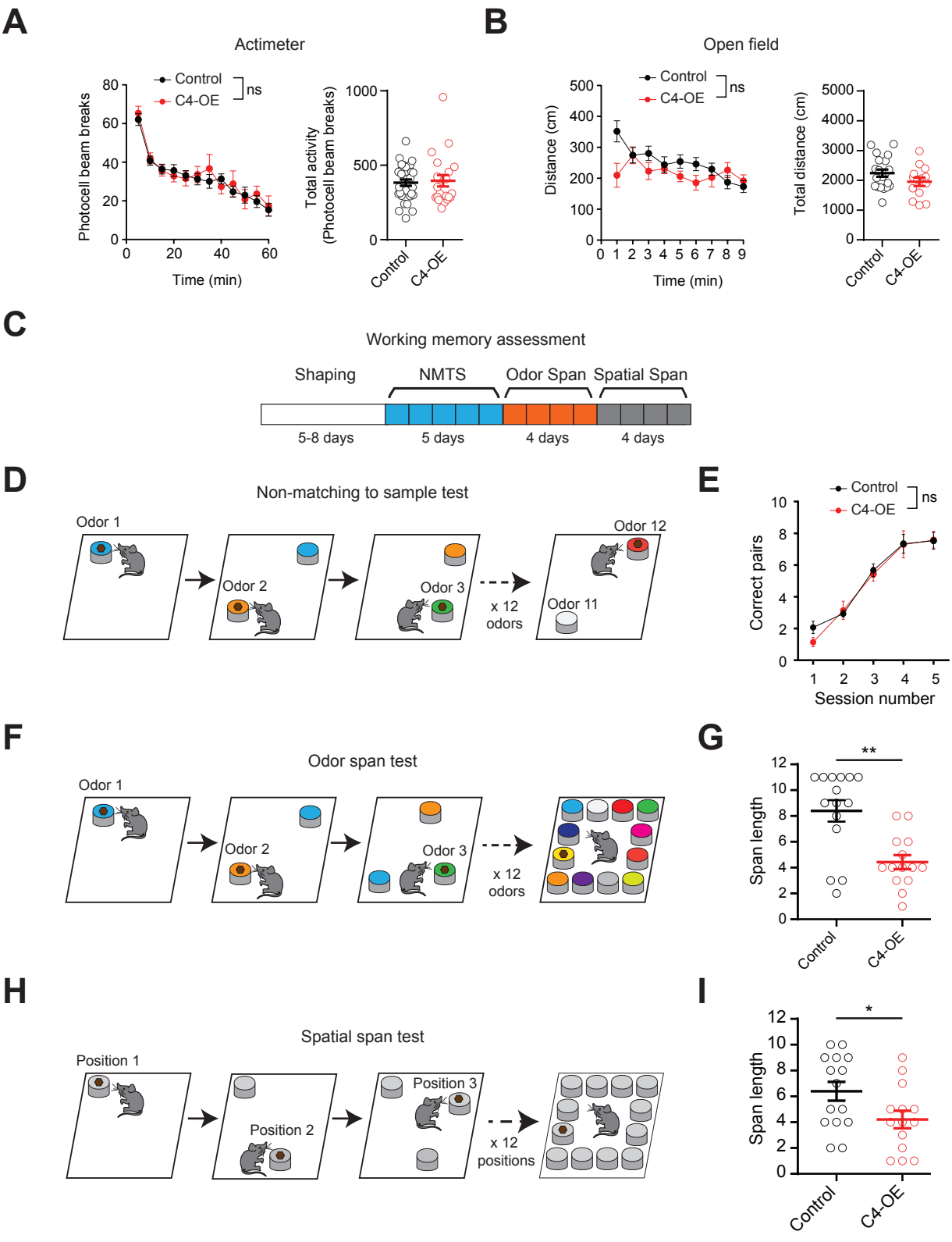
A
Actimeter
Control
C4-OE
ns
Photocell beam breaks
Time (min)
Total activity (Photocell beam breaks)
Control
C4-OE
B
Open field
Control
C4-OE
ns
Distance (cm)
Time (min)
Total distance (cm)
Control
C4-OE
C
Working memory assessment
Shaping
NMTS
Odor Span
Spatial Span
5-8 days
5 days
4 days
4 days
D
Non-matching to sample test
Odor 1
Odor 2
Odor 3
x 12 odors
Odor 11
Odor 12
E
Control
C4-OE
ns
Correct pairs
Session number
F
Odor span test
Odor 1
Odor 2
Odor 3
x 12 odors
G
**
Span length
Control
C4-OE
H
Spatial span test
Position 1
Position 2
Position 3
x 12 positions
I
*
Span length
Control
C4-OE

Supplementary Information

KEY RESOURCES TABLE

REAGENT or RESOURCE	SOURCE	IDENTIFIER
Antibodies		
Rat monoclonal anti-HA	Sigma	Cat# 11867431001; RRID: AB_390919
Rabbit anti-Parvalbumin	Swant	Cat# PV27; RRID: AB_2631173
Mouse monoclonal anti-Glutamate Decarboxylase 67	Millipore-Merk	Cat# G5419; RRID: AB_261978
Goat anti-rat Alexa Fluor 488	Invitrogen	Cat# A-11006; RRID: AB_2534074
Donkey anti-rabbit Cy3	Jackson ImmunoResearch	Cat# 711-165-152; RRID: AB_2307443
Goat anti-mouse Alexa Fluor 647	Jackson ImmunoResearch	Cat# 115-605-003; RRID: AB_2338902
Chicken anti-GAPDH	Millipore-Merk	Cat# AB2302; RRID: AB_10615768
Rabbit anti-C4 alpha Chain	Proteintech	Cat# 22233-1-AP; RRID: AB_2879042
Goat anti-chicken IR700	Advansta	Cat# R-05057-250; RRID: N/A
Goat anti-rat IR800	Advansta	Cat# R-05064-250; RRID: N/A
Goat anti-rabbit IR700	Invitrogen	Cat# 35568; RRID: AB_2633284
DNA and Plasmids		
C4b mouse sequence	NCBI Resources	NM_009780.2
pCAG-HAC4b	This paper	N/A
pCAG-TdTomato	This paper	N/A
Experimental Models: Organisms/Strains		
Mouse: C57Bl6/J	Janvier Labs	C57BL/6JRj
Mouse: PV-Cre (B6;129P2-Pvalb$^{tm1(cre)Arbr/J}$)	The Jackson Laboratory	JAX: 017320
Mouse: ChR2-YFP-loxP (B6;129S-Gt(ROSA)$^{26Sortm32(CAG-COP4*H134R/EYFP)Hze/J}$)	The Jackson Laboratory	JAX: 012569
Mouse: RCE-loxP (Gt(ROSA)$^{26Sortm1.1(CAG-EGFP)Fsh/Mmjax}$)	The Jackson Laboratory	JAX : 032037
Software and Algorithms		
GraphPad Prism	https://www.graphpad.com/	RRID: SCR_002798
ImageJ	https://imagej.nih.gov/ij/	RRID: SCR_003070
MiniAnalysis	http://www.synaptosoft.com/MiniAnalysis/	RRID: SCR_002184
IgorPro	https://www.wavemetrics.com/	RRID: SCR_000325
PatchMaster	http://www.heka.com/products/products_main.html#soft_pm	RRID:SCR_000034
NeuroMatic	http://www.neuromatic.thinkrandom.com/	RRID:SCR_004186
Imetronic	http://www.imetronic.com/	N/A
Viewpoint	https://viewpoint.fr/en/p/software/videotrack	N/A
Image Studio Lite	https://www.licor.com/bio/image-studio-lite/	RRID: SCR_013715

Materials and methods

Animals

All animal experiments were performed according to guidelines of the European Community for the use of animals in research and were approved by the local ethical committees (C2EA-05 in France; LANUV NRW in Germany). All experiments were performed on mice that had been electroporated at embryonic stage E15. Mice were housed in their home cages and kept under a 12-h light/dark cycle at 22 ± 2°C. Food and water were available ad libitum. For optogenetics experiments, we used electroporated transgenic Pvalb$^{tm1(cre)Arbr}$ $^{(+/-)}$::ChR2(H134R)-YFP$^{(lox/-)}$ mice obtained after crossing homozygous Pvalb$^{tm1(cre)Arbr}$ (JAX n°017320) females expressing Cre recombinase under the control of the Pvalb promoter (kindly provided by Dr JC Poncer, Institut du Fer à Moulin, Paris) and homozygous lox-STOP-lox ChR2-YFP males (JAX n°012569) (kindly provided by Dr MC Angulo, Institute of Psychiatry and Neuroscience, Paris). To identify and patch-clamp PV interneurons ex vivo, we used PV-Cre mice crossed with RCE:LoxP reporter mice (JAX n°010701) expressing enhanced green fluorescent protein (EGFP) under the control of the endogenous Gt(ROSA)26Sor promoter/enhancer regions and the CAG promoter. All mice were on a C57Bl/6J background. Females and males were used indifferently for electrophysiology, immunohistochemistry and imaging experiments. Only males were used for behavioral experiments.

DNA plasmid constructs

pCAG-HAC4 expression vector design was based on pCAG-HT2B-HA. The pCAG-HT2B-HA was a gift from I Moutkine (Fer à Moulin Institute, Paris). The HT2B gene was removed and replaced by the full coding sequence for murine C4b (NM_009780.2). The cDNA of C4b was obtained by reverse transcription PCR of total RNA from whole brain of adult 129S1/SvImJ mice. An HA tag was introduced at the N-terminus of the C4b sequence to allow the identification of the overexpressed C4 peptide. pCAG-tdTomato expression vector design was based on pCAG-mGFP which was a gift from Dr. C. Cepko [1] (Addgene plasmid # 14757). mGFP was replaced by tdTomato in the pCAG backbone. Subcloning of C4b and tdTomato sequences were done using InFusin (Clonetech) and DNA were purified with Nucleospin kit (Macherey-Nagel). All constructs were verified by sequencing the entire coding region of the inserts.

***In utero* electroporation**

Pregnant mice at E15 were anesthetized by isoflurane 4% and were injected with Flunixin (0.05mg/kg body weight) before surgery. The surgery was performed under isoflurane 2% on a heated blanket and breathing was carefully monitored during all the procedure.

A midline laparotomy was performed and the uterine horns were exposed and moistened with sterile NaCl 0.9%. Between 0.5µl to 1µl of a solution containing pCAG-C4HA vector (0.8 µg/µl) together with pCAG-TdTomato vector (0.4 µg/µl) (molar ratio 4:1) in NaCl 0.9% were injected into the bilateral ventricles with a glass micropipette made from a microcapillary tube (#5-000-1001-X10, Drummond Scientific). In the control condition, a solution containing pCAG-TdTomato (0.8 µg/µl) alone was injected. The injected plasmid solution contained Fast Green (0.1%) to monitor the injection. The embryo's head in the uterus was held between the tweezers-type electrode consisting of two disc electrodes of 5 mm diameter (CUY650P5, Nepagene). The cathode was placed just above the olfactory bulbs and the anode was placed at the back of the head below the cerebellum. Electrical pulses (50V; 50 ms) were applied five times at intervals of 950 ms with an electroporator (CUY21 Edit, Nepagene). The uterine horn was placed back into the abdominal cavity. The abdominal cavity was filled up with sterile NaCl 0.9% and the abdominal muscle and skin were sutured separately. After recovery, pregnant mice were returned to their home cage and sutures were exanimated every day until birth. Correct tdTomato expression was first checked through the intact skin shortly after birth (age P1-P2) and confirmed *post mortem* on brain slices from each experimental animal. Mice without tdTomato expression in the prefrontal cortex (PFC) were excluded from the analysis. Control and C4-OE electroporations were carried out in parallel (either on the same day or during the same week) in order to minimize experimental biases. The survival rate of electroporated control and C4-OE mice was comparable.

Cranial window surgery

At postnatal day 15 to 18 (P15-18) (and P30 respectively) a cranial window surgery was performed as previously described [2-4]. Mice were anesthetized with an intraperitoneal injection of ketamin/xylazin (0.13/0.01 mg/g body weight). For analgesia an additional subcutaneous injection of buprenorphin (0.05 mg/kg) was given. The anesthetic profile was deepened and maintained by inhalation of isoflurane (0.2-0.4% in 0.2 l/min oxygen). After the withdrawl reflex of the hind limb had subsided, the surgery begun. The eyes were covered with eye ointment (Bepanthen) to prevent drying and the mouse was placed on a heating pad

to maintain body temperature. Subsequently, mice were fixed to a stereotactic frame and the skin of the head was disinfected with 70% ethanol. The skin above the skull was removed using surgical scissors. To assure correct placement of the cranial window, the expression of the fluorophore was located using a UV light source. Next, the skull bone was dried and a 3 to 4-mm-diameter circular piece of bone was removed (3 mm at P15-P18, 4 mm at P30) over the prefrontal cortex using a dental drill. The dura mater was carefully removed and a circular coverslip (Ø 3mm at P15-P18, Ø 4 mm at P30) was inserted into the craniotomy and glued to the bone. The window was placed unilaterally above the electroporated hemisphere with the following coordinates describing the center of the circular glass (anteroposterior: +2mm, mediolateral: + or - 2mm (P30) and anteroposterior: +1.5 mm, mediolateral: + or - 1.5mm (P15-18). To allow stable and repetitive fixation of the mouse under the microscope, a small metal bar was attached next to the cortical window using UV-curable dental adhesive.

Two-photon *in vivo* imaging and analysis

Two-photon imaging was performed right after surgery at a Zeiss 7 multiphoton microscope with a Zeiss 20 x objective (NA = 1). The anesthesia was maintained with 1-1.5% inhalation of isoflurane while the mouse was head fixed to a custom-made imaging frame. 2P imaging was performed spanning a depth of 20-200 µm from the brain surface. This allowed us to image the full length of apical dendrites of Layer II/III pyramidal neurons. TdTomato fluorescence was excited at 980 nm using an InSight X3 tunable laser (Spectra-Physics) and collected through a 617/73 band-pass filter on a highly sensitive non-descanned detector. First, a 600 µm (x) x 600 µm (y) x 400 µm (z) overview z-stack (4 µm z-spacing) was acquired to retrieve the region of interest over multiple sessions. Then z-stacks of single dendrites (1 µm z-spacing) with a pixel size of 0.089 µm were acquired. After the first imaging session, the mice woke up and were placed in a cage with their littermates for 4-5 h (P15-18). For the second imaging session the mice were again anesthetized with isoflurane (initially 3%, then 1-1.5% for anesthesia maintenance) and imaged to retrieve the same dendritic structures recorded in the first imaging session.

Datasets were blinded prior to analysis by an experimenter not involved in the image analysis. In each animal 4-19 dendrites of 30-120 µm length were analyzed. Spines that extended out laterally from the dendritic shaft were counted manually by scrolling through the z-stack, as previously described[5]. Spine density was calculated by the number of spines divided by the

length of the respective dendrite. Turnover of dendritic spines was calculated as follows: turnover [%] = 100*((#gained + #lost)/(#T1+#T2)). Here, #gained refers to the number of gained and #lost to the number of lost spines, respectively and #T1 and #T2 to the number of all spines at time-points T1 and T2, respectively. T1 and T2 refer to 0h and 4h.

Confocal imaging of dendritic spines and analysis

Tissue preparation and immunochemistry

All mice were injected with a lethal dose of pentobarbital (200 mg/kg) and perfused transcardially with saline solution followed by 4% (w/v) paraformaldehyde in phosphate buffered saline. Brains were removed, post-fixed in 4% paraformaldehyde for 20 hours, and then sectioned at 50 μm in the coronal plane using a vibratome (VT1200, Leica). Sections were mounted (Dako Fluorescence mounting medium) directly on coverslips for confocal imaging.

Fixed tissue imaging

Images of fixed brain slices were acquired on a commercial confocal microscope equipped with an Airyscan detector (Zeiss LSM800, Carl Zeiss Microscopy GmbH, Jena, Germany), using a 63X/1.4NA oil objective. Excitation of tdTomato was achieved by a 561nm laser and emission was collected using a 565-700 nm bandpass filter. Image stacks of dendrite fragments of pyramidal neurons were acquired with a pixel size of 0.049 μm, a z-step size of 0.200 μm and at a scan speed of 2.55 μs/pixel. Images acquired with the Airyscan detector were processed by the ZEN software internal algorithm that reassigns the collected pixels to their correct positions to achieve a super-resolution image; for this a super-resolution threshold of 2 was used.

Reconstruction of dendritic fragments

Image stacks were 3D reconstructed in IMARIS x64 8.1.2 (Bitplane AG, Zurich). Basal and apical dendrites and their associated spines were reconstructed semi-automatically using the Filament Tracer module. Spines that extended radially from the dendrite in three dimensions were drawn manually by turning the 3D visualized dendritic fragment.

Filament parameters, that is small diameter = 0.08 μm, large diameter = 0.80 μm and contrast threshold = 0.10 were defined empirically by measuring a random set of acquired images and comparing the rendered filament with the preprocessed image. Spine density per dendritic fragment and morphological parameters of spines (ratio of mean head to neck diameter,

maximum head diameter and spine length) were measured, exported for further analysis (Cluster analysis) and plotted in a 3D graph.

Cluster analysis

The cluster analysis was performed as previously described[6]. The spine parameters, ratio of the mean head to neck diameters (ØHead/ØNeck), the maximum head diameter (Ømax Head) and spine length were taken into account. Agglomerative Hierarchical Clustering Analysis (AHC) was performed using Python's scikit-learn toolbox. Before cluster analysis, the parameters were centered and scaled to unit variance using the standard scaler from Python's scikit-learn toolbox. AHC dissimilarity level was calculated based on Euclidean distance. Agglomeration was performed using Ward's method. By fitting the hierarchical clustering to the population of all analyzed spines we identified three clusters.

Histology

Immunohistochemistry

Mice aged P30 and P180 were anesthetized with pentobarbital (150 mg/kg) and intracardially perfused with PBS followed by 4% buffered formaldehyde (Histofix, Roti). The brains were removed and fixed overnight in 4% Histofix. 40 µm sagittal sections were cut using a vibratome (VT1000S, Leica). Free-floating sections were permeabilized and blocked in 0.2% Triton-PBS, 3% BSA-PBS for 60 min before incubation with the first antibody in 0.2% Triton, 3% BSA-PBS overnight at 4°C. After three washes in PBS, sections were incubated with the secondary antibody in PBS for 2h, washed again in PBS, and mounted using Fluoromount G (Invitrogen). Primary antibodies were: rat anti-HA (1:300, Sigma), rabbit anti-Parvalbumin (PV27, 1:1000, Swant), mouse anti-Glutamate Decarboxylase 67 (GAD67, clone 1G10.2, 1:500, Millipore-Merk). Secondary antibodies were: goat anti-rat Alexa Fluor 488 (1:400, Invitrogen), donkey anti-rabbit Cy3 (1:1000, Jackson Immuno Research), goat anti-mouse Alexa Fluor 647 (1:1000, Jackson Immuno Research). Hoechst 33342 was used for nuclear staining. Images were acquired using a confocal microscope (SP5, Leica).

PV cell number and distribution

The distribution of PV neurons in different PFC layers was quantified using maximal intensity projections of 3D confocal stacks. For each mouse, 4 PFC sagittal sections were imaged using a confocal microscope (Leica SP5, 40X objective). Layers were identified based on Hoechst nuclear staining and delineated using ImageJ's ROI manager software. The

distribution of PV neurons in different PFC layers was quantified using maximal intensity projections of 3D confocal stacks. The density of PV cells (number of PV cells per surface unit) in each layer was obtained by averaging the density across the 4 slices. During image acquisitions and quantifications, the investigator was blind to the condition (control or C4-OE).

GAD67 expression

GAD67 expression levels in PV cells were measured by analyzing confocal images (Leica SP5, 40X objective) using ImageJ. For each animal, 3 to 4 PFC sagittal slices were acquired. At least 80 PV neurons per mouse were analyzed. A single confocal section located 10 µm below the surface of the slice was acquired in each slice. The same acquisition parameters were used for each slice and were set such that the brightness of the GAD67 immunostaining was below saturation values. The brightness of the PV immunostaining was set above saturation level, allowing to use PV as a marker to delineate the shape of PV neurons. The density of GAD67 immunostaining within PV cells was then automatically calculated using Image J. Several experiments were performed with a minimum of 6 mice per condition. As the fluorescence intensity is only comparable for samples processed simultaneously, the results are presented as a percentage of the mouse controls performed at the same time. During image acquisitions and quantifications, the investigator was blind to the condition (control or C4-OE).

Acute slice preparation

250 µm-thick coronal slices were prepared from brains of control and C4-OE mice. Mice were deeply anesthetized with sodium pentobarbital (150 mg/kg) and perfused transcardially with ice-cold (0–4°C) oxygenated (95% O_2-5% CO_2) solution containing (in mM): 110 Choline chloride, 2.5 KCl, 25 glucose, 25 NaHCO3, 1.25 NaH2PO4, 0.5 CaCl2, 7 MgCl2, 11.6 L-ascorbic acid and 3.1 sodium pyruvate. The brain was extracted and acute sagittal slices were cut in the same ice-cold solution using a vibroslicer (HM 650 V, Microm), then stored in artificial cerebrospinal fluid (ACSF) containing the following (in mM): 125 NaCl, 2.5 KCl, 25 glucose, 25 NaHCO3, 1.25 NaH2PO4, 2 CaCl2, and 1 MgCl2, continuously bubbled with 95% O_2-5% CO_2. Slices were incubated in ACSF at 32°C for 20 minutes and then at room temperature (20-25°C). For patch-clamp recordings, slices were transferred to the recording chamber where they were continuously superfused with ACSF (30-32°C) buffered by continuous bubbling with 95% O_2-5% CO_2.

Electrophysiology and optogenetics

Whole-cell current and voltage-clamp recordings were performed in PFC layer II/III. Recorded pyramidal cells all expressed tdTomato. Recorded PV interneurons were in the vicinity of electroporated tdTomato+ pyramidal cells and were visually identified based on the expression of EGFP (in PV-Cre::RCE mice) or YFP (in PV-Cre::lox-STOP-lox ChR2-YFP mice). Stimulus delivery and data acquisition were performed using Patchmaster software (Multichannel Systems). Signals were acquired with an EPC10-usb amplifier (Multichannel Systems), sampled at 20 kHz and filtered at 4 kHz. Offline analysis was performed using Clampfit (Molecular Devices) and Igor Pro (Wavemetrics). For the study of miniature post synaptic currents, recordings were filtered offline at 2 kHz and analyzed using MiniAnalysis (Synaptosoft).

Patch-clamp pipettes (3–6 Mohm resistance) were prepared from borosilicate glass (BF150-86-10; Harvard Apparatus) using a DMZ pipette puller (Zeitz). Current-clamp experiments were performed using the following intracellular solution (in mM): 105 K-gluconate, 10 HEPES, 10 phosphocreatine-Na, 0.3 Na3GTP, 4 MgATP, 30 KCl (pH 7.25, adjusted with KOH). For voltage-clamp experiments the following intracellular solution was used (in mM): 120 Cs-methane sulfonate, 10 CsCl, 10 Hepes, 10 Phosphocreatine, 0.2 EGTA, 8 NaCl, 2 ATP-Mg, 3 QX 314 (pH 7.25, adjusted with CsOH). To record miniature and evoked inhibitory postsynaptic currents (mIPSCs ans eIPSCs), we used an intracellular solution containing (in mM): 60 Cs methane sulfonate, 70 CsCl, 10 Hepes, 10 Phosphocreatine, 0.2 EGTA, 8 NaCl, 2 ATP-Mg (pH 7.25, adjusted with CsOH). Liquid junction potentials (-14.9 mV for Cs-based intracellular solutions and -5mV for the K+-based intracellular solution) were left uncorrected. The cell membrane resistance, membrane capacitance and series resistance were calculated in the seal-test configuration from the decay and steady-state of a current generated in response to a 10 mV hyperpolarizing voltage step. The series resistance was left uncompensated.

Excitability

Pyramidal cell and PV interneuron intrinsic properties and excitability were recorded in current-clamp in presence of the following synaptic blockers: SR95531 hydrobromide (Gabazine, 10 μM, Hello Bio), 6-cyano-7-nitroquinoxaline-2,3-dione (CNQX, 10 μM, Hello Bio) and D-2-amino-5-phosphonopentanoic acid (D-APV, 50 μM, Hello Bio). Spike frequency-depolarization curves were generated by injecting series of 500 ms depolarizing current steps increasing by 50 pA. The firing pattern of patched-clamped YFP+ cells in the

cortex of PV-Cre::lox-STOP-lox ChR2-YFP mice was monitored using 500 ms pulse of blue light emitted by a light emitting diode (CoolLED).

Miniature EPSCs and evoked EPSCs

Miniature excitatory post synaptic currents (mEPSCs) were recorded at a holding potential of -65 mV in the presence of tetrodotoxin (TTX, 0.5 μM, Hello Bio) and Gabazine (10 μM). At least 100s were analysed for each recording. Evoked excitatory post synaptic currents (eEPSCs) were recorded at a holding potential of -65 mV and triggered at a frequency of 0.1 Hz in the presence of GABAzine (10 μM) with a monopolar electrode connected to a constant current stimulator (Iso-Flex, A.M.P.I.), positioned in the vicinity of the recorded neuron. At least 12 consecutive sweeps were acquired for each cell. The paired-pulse ratio (PPR) was calculated as the ratio of the peak amplitude of the averaged current response evoked by the second stimulation to the peak amplitude of the averaged current response evoked by the first stimulation.

Miniature IPSCs and evoked IPSCs

mIPSCs were recorded at a holding potential of -65 mV in the presence of TTX (0.5 μM, Hello Bio), CNQX, (10 μM) and D-APV (50 μM). At least 100 s were analysed for each recording. Evoked IPSCs were recorded at a holding potential of +10mV to avoid unclamped action potentials commonly associated with evoked IPSCs measured at hyperpolarized potentials in our high-chloride recording conditions, in the presence of CNQX (10 μM) and APV (50 μM). At least 25 consecutive sweeps were acquired and averaged for each cell. For electrically evoked IPSC (eIPSCs), four stimulations at 20 Hz were applied with a monopolar electrode connected to a constant current stimulator positioned in layer 3, 100-150 μm away from of the recorded neuron. For light-evoked IPSCs, the recorded pyramidal cell was placed in the center of the field of view. The response to four 0.5-ms pulses of blue light (470nm) at 20 Hz emitted by a light emitting diode (CoolLED) was recorded. The paired-pulse ratio of eIPSCs was calculated as the ratio of the peak amplitude of the averaged current response evoked by the second, third and fourth stimulations to the peak amplitude of the averaged current response evoked by the first stimulation.

AMPA/NMDA ratio and rectification index of AMPAR-mediated currents

To measure the AMPA/NMDA ratio and the rectification index, EPSC were evoked with a monopolar electrode positioned in layer 3, 100-150 μm away from the recorded neuron. At

least 12 consecutive sweeps were acquired and averaged at each holding potential. The AMPA/NMDA ratio was recorded in presence of GABAzine (10 μM). The AMPA current (I_{AMPA}) was measured as the peak amplitude of the current response at a holding potential of -65mV. The NMDA current (I_{NMDA}) was measured at a holding potential of +55mV, 50ms after stimulation, when AMPAR-mediated current have receded due to the fast deactivation kinetics of AMPARs. The ratio is calculated as I_{AMPA}/I_{NMDA}.

To study the rectification AMPA-mediated currents, pyramidal cells were recorded in the presence of GABAzine (10 μM) and D-APV (50 μM). Spermine (10 μM) was added to the intracellular solution. The rectification index was defined as the peak amplitude of synaptic currents measured at a holding potential of +55 mV (≈ +40 mV after correcting for junction potential) multiplied by 2 and divided by the peak amplitude of synaptic currents measured at a holding potential of -65mV (≈ -80 mV after correcting for junction potential).

Behavior

Actimeter

We used actimeter racks of 8 circular corridors (Imetronic, http://www.imetronic.com/devices/circular-corridor/) equipped with infrared sensors to detect and automatically record locomotion. Animals were introduced individually in corridors and their spontaneous, novelty-driven activity was recorded for a total of 60 minutes. Activity, measured as photocell beam breaks, was averaged over periods of 5 minutes. Control and C4-OE male mice were tested at weaning (age P30).

Open Field

The test took place in a white open-field apparatus (ViewPoint, Lyon, France) under high illumination (~100 lux). Animal were individually placed in the corner of the open-field and were allowed to explore for 9 min. A video tracking system, which included a computer-linked overhead camera, was used to monitor general lon comotor activity (https://viewpoint.fr/en/p/software/videotrack, ViewPoint, Lyon, France). Control and C4-OE male mice were tested a week after weaning (age P35 – P39).

Odor Span and Spatial Span Test

Working memory capacity was tested using a protocol adapted from a previous study [7]. All scented mixtures were prepared with 100 g of sawdust, 18 ground powdered pellets

(Chocapic, Nestle) to mask the scent of the reward pellet and 3 g of a ground powder odor (Savory, Cinnamon, Cumin, Nutmeg, Mint, Fennel, Four spices, Herbs of Provence, Coriander, Basil, Coffee, Ginger). During shaping and testing, adult (4- to 6-month-old) male mice were maintained at 80-85% of their body weight. During the shaping phase, mice were trained to dig into a bowl of unscented sawdust to retrieve the hidden reward pellet. Once all animals had learned the procedure, the non-matching to sample (NMTS) task started for 5 consecutive days. Each day, the mouse was placed on a square platform and required to dig into the first bowl (odor 1) to retrieve the reward and to remember the scent of that bowl. Upon consumption of the reward pellet, a second baited bowl (odor 2) was added. The first bowl (no longer baited) and the new bowl were randomly distributed on the platform. Following retrieval of the pellet, the first bowl was removed and a novel baited bowl (odor 3) randomly placed. This process was repeated until each individual mouse had been exposed to 11 pairs of scented bowls or stopped after a maximum of 12 minutes when the mouse did not perform the task, and the number of correct pairs (direct digging into the baited bowl) was recorded. The order of the odors was randomized across days.

Following the NMTS, animals were then tested 4 consecutive days for the odor span task, using the same procedure except that, following reward retrieval, the no longer baited bowls were not removed so that mice had to remember an increasing numbers of odors (span). The span length was calculated as the number of correct responses with more than one bowl on the platform prior to the first mistake. Thus, using 12 odors, the maximum span length is 11. The span score was given by the first mistake, but each mouse was allowed to continue the task until the 12 odors had been sampled or for a maximum of 12 minutes. The span length was the best score obtained by each tested mouse over a period of 4 consecutive days. As for the NMTS task, the order of the odors was randomized across days.

The same mice were subsequently tested for 4 consecutive days in the spatial span task. They had to remember an increasing numbers of locations, following a procedure similar to the odor span test, except that bowls of unscented sawdust were identified according to their spatial location on the platform. The span length was the best score obtained by each tested mouse over a period of 4 consecutive days.

The investigator was blind to the condition (control or C4-OE) during behavioral tests and analysis.

Immunoblotting

Mice were euthanized under anesthesia and brains were removed from the skull. TdTomato-expressing areas of the prefrontal cortex were dissected under a stereomicroscope. Extracts were lysed in RIPA buffer (50 mM Tris, pH 8.0, 150 mM NaCl, 10 µl/ml NP-40, 5 µg/ml sodium deoxycholate, 1 µg/ml SDS) containing Complete protease inhibitors (Roche). 10 brain extracts in each condition were pooled and equal amounts of proteins (60µg) were loaded on NuPAGE 8–12% Bis-Tris gels (Thermo Fisher Scientific) and transferred to 0.45 µm nitrocellulose membrane in 25 mM Tris–HCl, pH 7.4, 192 mM glycine and 200 ml/l ethanol for 2h at 4°C. Membranes were blocked with 50 g/l non-fat dry milk in Tris-buffered saline (TBS; 0.25 M Tris/0.5 M NaCl, pH 7.5) for 1 h at room temperature and then incubated with primary antibodies in the same buffer containing Tween 0.1% (TBST) for at least 2h. After three washes in TBST, the membranes were incubated for 1h with IRDye-conjugated secondary antibodies, and imaged using Odyssey Imaging System (LI-COR Biosciences). Quantifications were performed using Image Studio Lite software (LI-COR Biosciences). C4 levels were quantified by normalizing to the loading control, GAPDH. Primary antibodies were: rat anti-HA (1:500, Sigma), rabbit anti-C4α (1:2000, Proteintech), chicken anti-GAPDH (1:2000, Millipore). Secondary antibody were: goat anti-rat IR800 (1:10000, Advansta), goat anti-rabbit IR700 (1:10000, Invitrogen) and goat anti-chicken IR700 (1:10000, Advansta).

Statistical analysis

Data are presented as mean ± SEM. Statistical analyses were performed using Prism (Graphpad). The normality of data distribution was tested using Shapiro-Wilk's test. Unpaired two-tailed T-tests (for normally distributed datasets) or Mann–Whitney tests (for non-normally distributed datasets) were used for comparisons between two groups. For multiple comparisons we used two-way ANOVA followed by Sidak's test. Values of $P < 0.05$ were considered statistically significant. P values are reported as follows: * $P < 0.05$; ** $P < 0.01$; *** $P < 0.001$; **** $P < 0.0001$.

Supplementary references

1. Matsuda T, Cepko CL. Electroporation and RNA interference in the rodent retina in vivo and in vitro. *Proc Natl Acad Sci U S A* 2004; **101**(1)**:** 16-22.

2. Bittner T, Fuhrmann M, Burgold S, Ochs SM, Hoffmann N, Mitteregger G *et al.* Multiple events lead to dendritic spine loss in triple transgenic Alzheimer's disease mice. *PLoS One* 2010; **5**(11)**:** e15477.

3. Fuhrmann M, Bittner T, Jung CK, Burgold S, Page RM, Mitteregger G *et al.* Microglial Cx3cr1 knockout prevents neuron loss in a mouse model of Alzheimer's disease. *Nat Neurosci* 2010; **13**(4)**:** 411-413.

4. Fuhrmann M, Mitteregger G, Kretzschmar H, Herms J. Dendritic pathology in prion disease starts at the synaptic spine. *J Neurosci* 2007; **27**(23)**:** 6224-6233.

5. Gu L, Kleiber S, Schmid L, Nebeling F, Chamoun M, Steffen J *et al.* Long-term in vivo imaging of dendritic spines in the hippocampus reveals structural plasticity. *J Neurosci* 2014; **34**(42)**:** 13948-13953.

6. Pfeiffer T, Poll S, Bancelin S, Angibaud J, Inavalli VK, Keppler K *et al.* Chronic 2P-STED imaging reveals high turnover of dendritic spines in the hippocampus in vivo. *eLife* 2018; **7**.

7. Young JW, Kerr LE, Kelly JS, Marston HM, Spratt C, Finlayson K *et al.* The odour span task: a novel paradigm for assessing working memory in mice. *Neuropharmacology* 2007; **52**(2)**:** 634-645.

8. Gabbott PL, Warner TA, Jays PR, Salway P, Busby SJ. Prefrontal cortex in the rat: projections to subcortical autonomic, motor, and limbic centers. *J Comp Neurol* 2005; **492**(2)**:** 145-177.

9. Schwab M, Agid Y, Glowinski J, Thoenen H. Retrograde axonal transport of 125I-tetanus toxin as a tool for tracing fiber connections in the central nervous system; connections of the rostral part of the rat neostriatum. *Brain Res* 1977; **126**(2)**:** 211-224.

10. Arikuni T, Kubota K. The organization of prefrontocaudate projections and their laminar origin in the macaque monkey: a retrograde study using HRP-gel. *J Comp Neurol* 1986; **244**(4)**:** 492-510.

11. Reiner A, Hart NM, Lei W, Deng Y. Corticostriatal projection neurons - dichotomous types and dichotomous functions. *Front Neuroanat* 2010; **4:** 142.

Supplementary figures, tables and legends

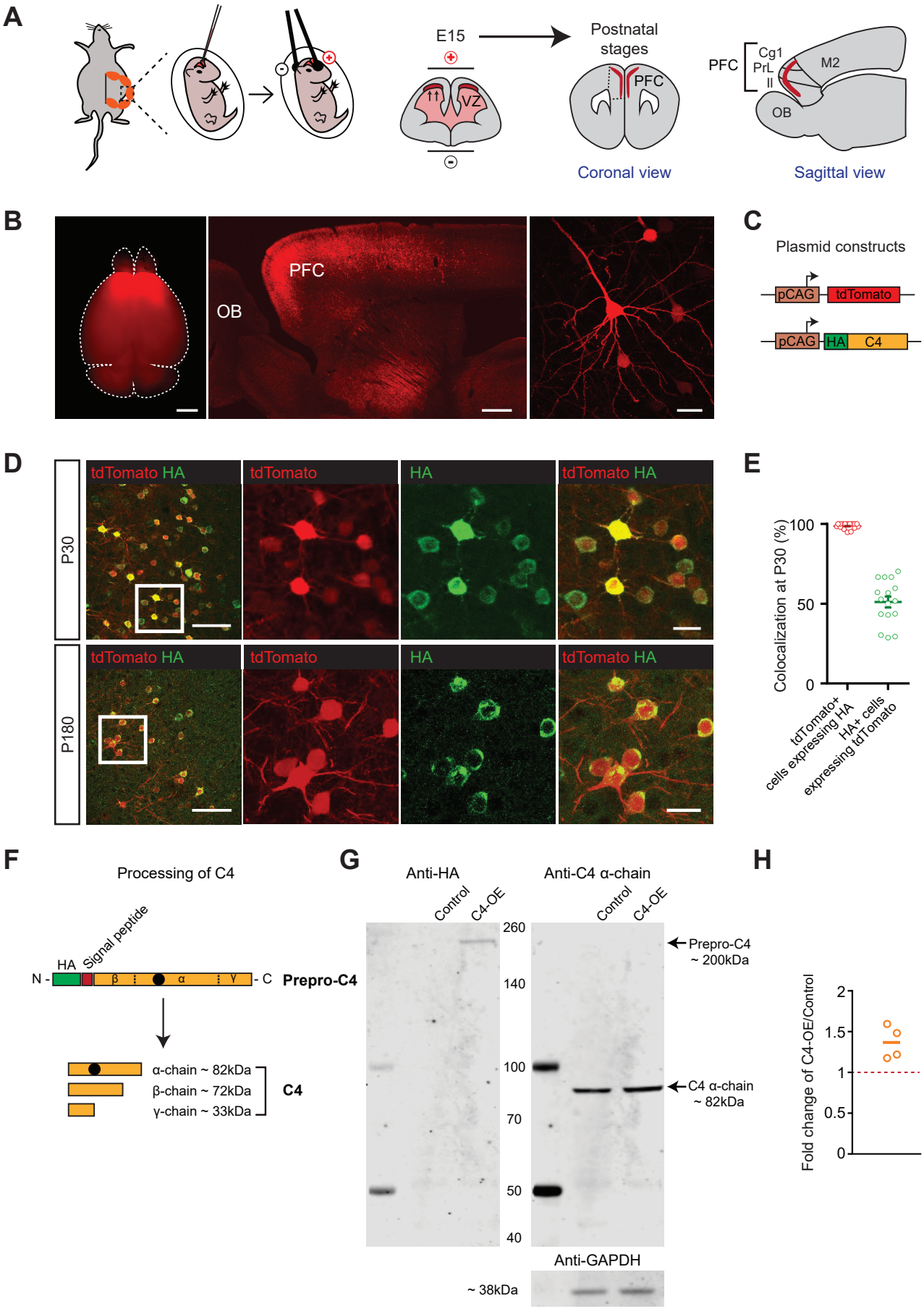

Supplementary Figure 1: C4 overexpression in prefrontal cortex using in utero electroporation

(A) Schematic drawing illustrating the in utero electroporation (IUE) method at embryonic day 15 (E15) for specific targeting of layer II/III PFC pyramidal neurons. Targeted PFC areas include the anterior cingulate cortex (Cgl), the prelimbic cortex (PrL) and the infralimbic cortex (Il). VZ: ventricular zone; OB: olfactive bulb.

(B) Left panel: Electroporated brain at postnatal day 30 (P30) exhibiting tdTomato expression in PFC; scale bar: 5 mm. Middle panel: Sagittal slice showing the distribution of TdTomato positive cells in PCF layer II/III. Note that the expression of tdTomato in the striatum originates from tdTom+ PFC neurons in layer II-III which are known to send direct axonal projections to the striatum in mammals8-11. OB: olfactive bulb; scale bar: 500 µm. Right panel: typical morphology of an electroporated pyramidal cell; scale bar: 30 µm.

(C) Plasmid constructs used for IUE. Embryonic brains were co-electroporated with pCAG-HA-C4 and pCAG-tdTomato for C4 overexpression (C4-OE), or only with pCAG-tdTomato (control). pCAG-HA-C4 and pCAG-tdTomato were co-electroporated with a 4:1 ratio to ensure that most tdTomato+ cells overexpressed C4.

(D) Immunostaining for TdTomato (red) and HA (green) in PFC layer II/III at P30 (upper panels) and P180 (bottom panels). The three panels on the right are enlargements of the boxed area in the left panel. Note that tdTom+ neurons also expressed HA-C4; scale bar: 100 µm; scale bar in magnified image: 20 µm.

(E) Quantification of the results obtained from P30 mice as exemplified in (D).

(F) Schematic drawing illustrating the processing of C4: C4 is synthesized as a single chain precursor molecule (prepro-C4) and processed to a three-chain structure (β−α−γ) before secretion. The HA tag was added at the 5' end of the signal peptide-encoding sequence, i.e. before the signal peptide region, in order not to interfere with the folding and processing of C4. The black dot represents the antigenic region recognized by the anti-C4 α-chain antibody used for western blot experiments in (G).

(G) Immunoblot of HA (left) and C4 α-chain (right) in lysates from the electroporated region of control and C4-OE mice aged P30. To compensate for the lack of material and relatively low levels of C4 expression, lysates from the electroporated region were prepared from individual mice and pooled for the western blot analysis (control mice: N = 10 ; C4-OE mice: N = 10). Left panel: HA was only detected at the molecular weight of prepro-C4 (~ 200 kDa) in the C4-OE condition, suggesting that the HA tag was correctly cleaved together with the signal peptide. Right panel: a band was detected at the molecular weight of the C4 α-chain (~ 93 kDa). Data were normalized to GAPDH.

(H) Densitometry quantification of the results illustrated in (G). Data were normalized to GAPDH for each experiment and expressed as a fold change of control mean density. The experiment was repeated four times. Each circle represents the result of an individual experiment. The bar represents the mean of four experiments.

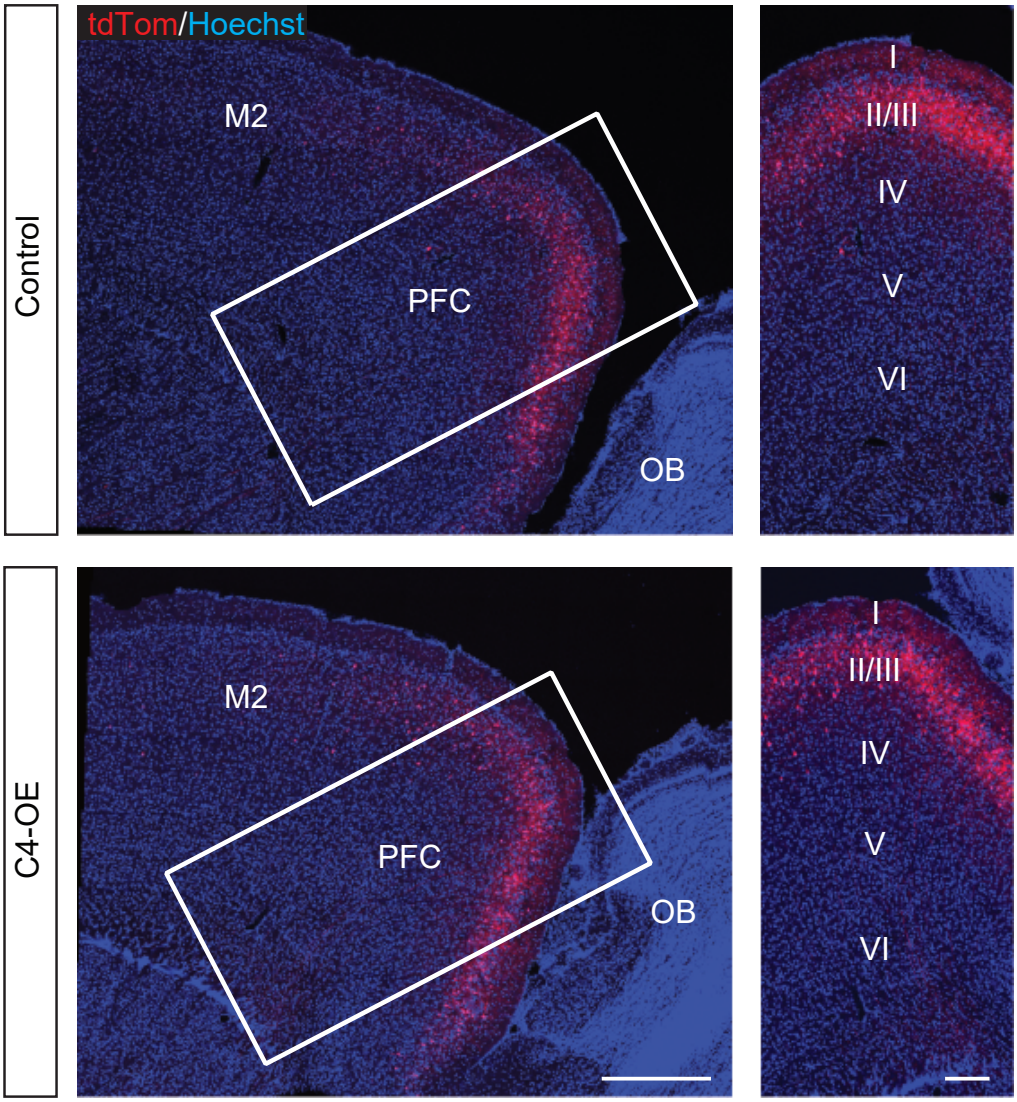

Supplementary Figure 2: Similar laminar position of electroporated pyramidal cells in control and C4-OE mice

Left: sagittal PFC sections from control and C4-OE mice; scale bar: 300µm. Right, enlargements of the boxed area in the left panel showing PFC layers. All tdTomato+ cells are located in PFC layer III; scale bar: 100 µm; M2: motor cortex; PFC: prefrontal cortex; OB: olfactory bulb.

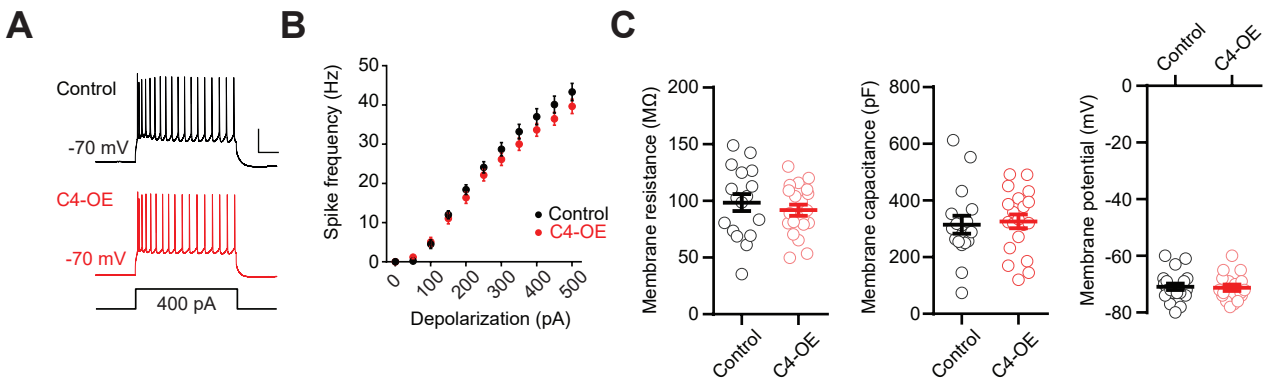

Supplementary Figure 3: Passive and active neuronal properties in control and C4-OE mice

(A) Sample spike trains evoked by a 400 pA somatic current injection in a control and in a C4-OE pyramidal cell; scale bars: 20 mV/100 ms.

(B) f-i curves for control (n = 20 cells from 3 mice) and C4-OE neurons (n = 17 cells from 3 mice).

(C) Input resistance (left), Cell capacitance (middle) and resting membrane potential (right) in control (n = 20 cells from 3 mice) and C4-OE neurons (n = 17 cells from 3 mice). Neither firing frequency nor intrinsic neuronal properties differed between control and C4-OE pyramidal cells.
All data are represented as mean ± SEM. Each open circle represents an individual neuron.

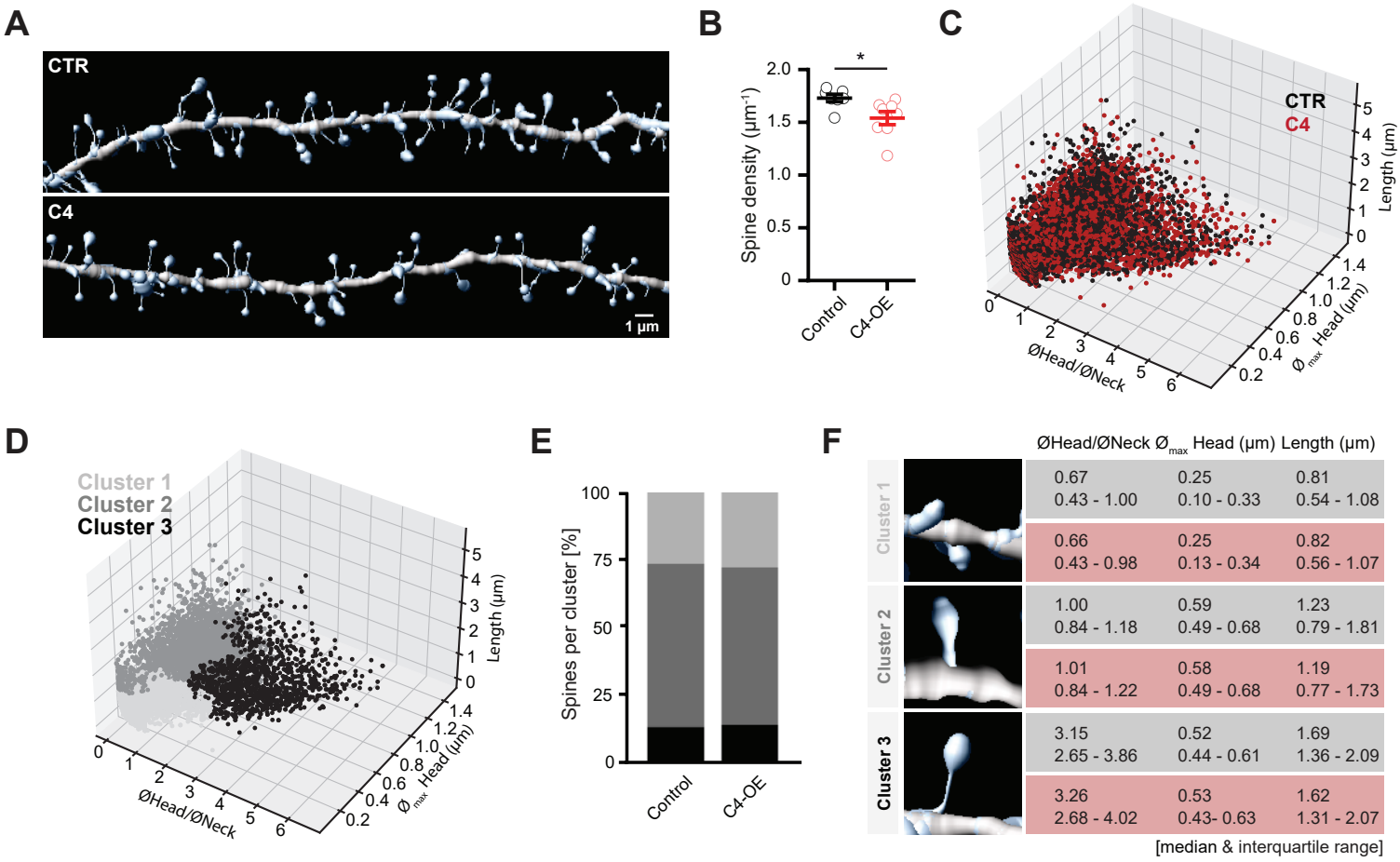

Supplementary Figure 4: Cluster analysis of dendritic spines in control and C4-OE mice

(A) 3D reconstruction of dendritic fragments confocally imaged in fixed tissue of control (CTR) and C4-OE animals aged P15-P18.

(B) Spine density measured on reconstructed dendrites; data from n = 7 CTR and n=8 C4-OE mice with in total 49 (CTR) and 66 (C4-OE) dendrites; single dots show individual mice; diagram shows mean ± SEM; p=0.0229, unpaired t-test; statistics were performed using individual mice as the unit of analysis.

(C, D) 3D morphology plots visualizing the spines of CTR and C4-OE mice (C), and their affiliation to identified clusters 1, 2 and 3 (D); plotted are, the ratio of mean head to neck diameters (ØHead/ØNeck), spine length and maximum head diameter (Ømax Head) of in total 8123 (CTR) and 10946 spines (C4-OE).

(E) Quantification of spine proportions within identified clusters, comparing spines of CTR and C4-OE mice.

(F) Table summarizing the morphological parameters utilized for the cluster analysis: ØHead/ØNeck, Ømax Head and length of spines, for CTR (grey) and C4-OE animals (red). Data are represented as median and interquartile range (25th–75th percentile).

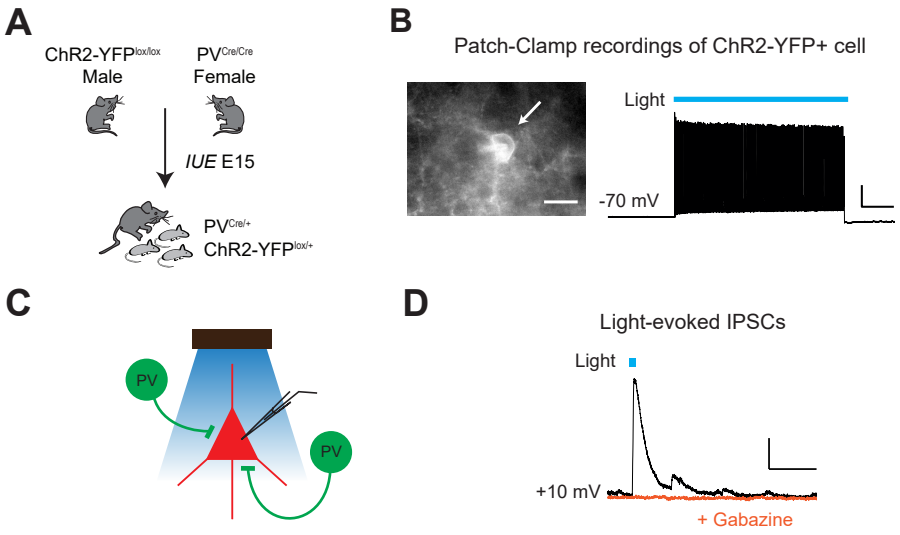

Supplementary Figure 5: Light-evoked firing of ChR2-expressing PV neurons

(A) Homozygous PV-Cre::RCE females were crossed with homozygous lox-STOP-lox ChR2-YFP males before electroporation of timed-pregnant females with tdTomato or C4 + tdTomato. Electroporated offspring (age P25-P30) were used for ex vivo patch-clamp and optogenetics.

(B) Left, patch-clamped YFP+ cell (arrow); right, spike train evoked by a 500 ms pulse of blue (470 nm) light. YFP+ cells exhibited the typical fast-spiking pattern of PV neurons (n = 3 neurons).

(C) Light-evoked IPSCs were recorded at a holding potential of +10 mV in electroporated PFC pyramidal cells from control or C4-OE PVCre-RCE::lox-STOP-lox ChR2-YFP mice.

(D) Light-evoked IPSC blocked by the addition of of Gabazine (10 μM), demonstrating its GABAergic nature; scale bars: 50 pA/50ms.

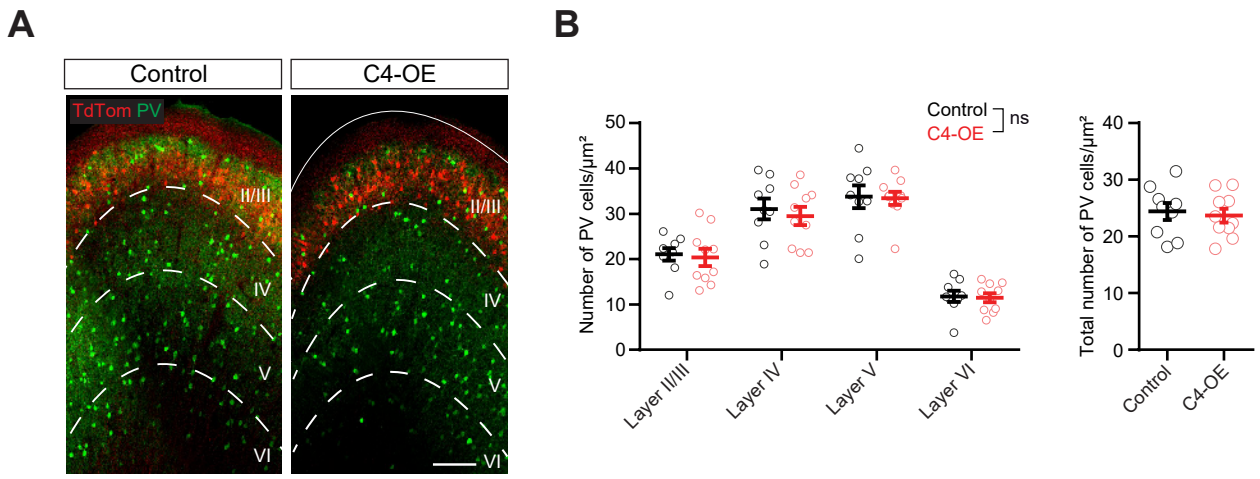

Supplementary Figure 6: Laminar distribution of PV neurons in control and C4-OE mice

(A) PV staining in PFC sagittal slices from a control and from a C4-OE mouse; scale bar: 100 µm.

(B) The repartition by layer (left) as well as the total number of histologically identified PV (right) was unchanged in C4-OE mice (n = 10 mice) compared to control mice (n = 9 mice) (Two-Way ANOVA, $P > 0.05$). All data are represented as mean ± SEM. ns, not significant.

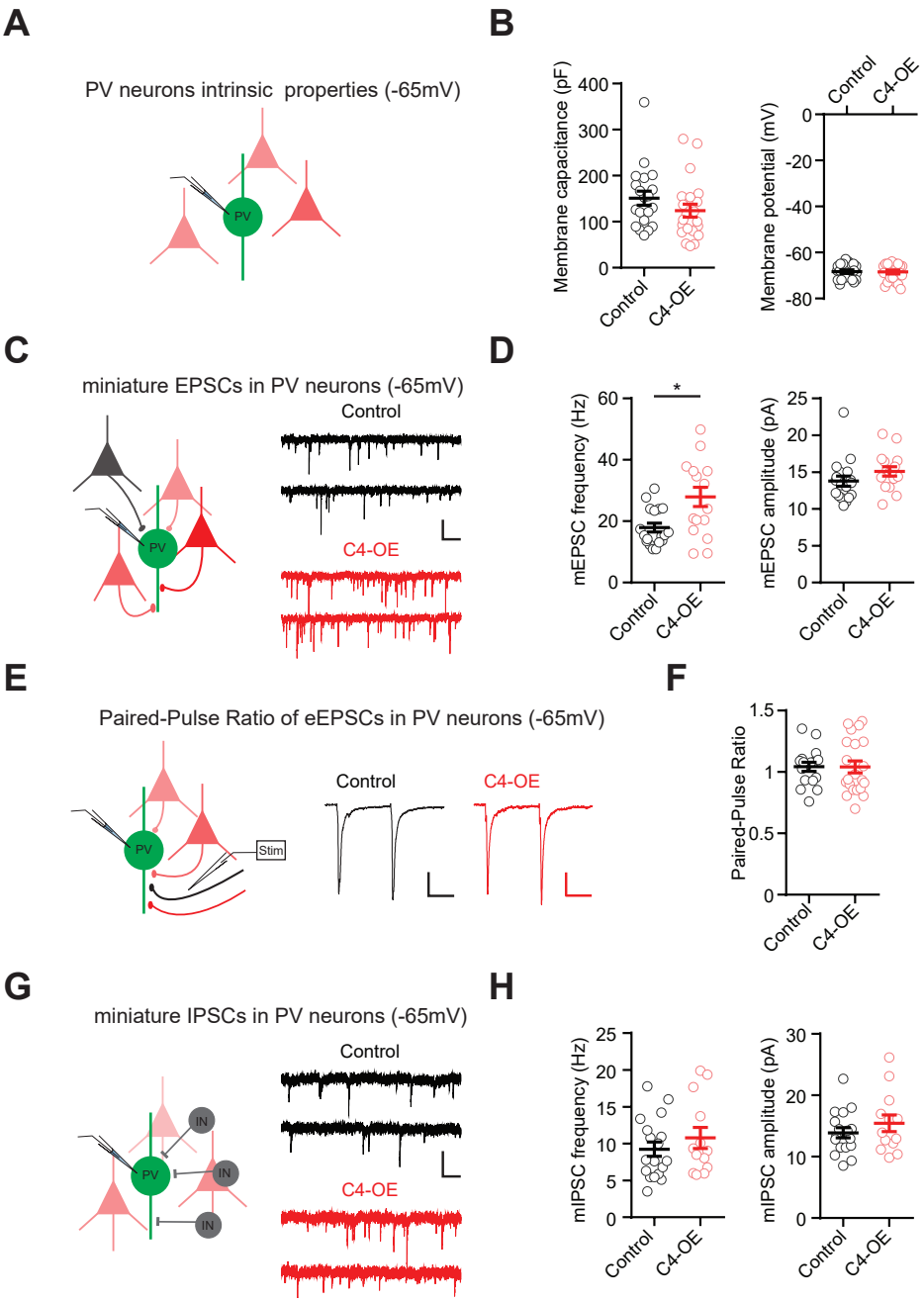

Supplementary Figure 7: Increased excitatory inputs onto PV neurons in C4-OE mice

(A) Sample traces of mEPSCs recordings in PV interneurons from control and C4-OE juvenile (P25-P30) mice recorded at −65 mV in the presence of TTX and GABAzine; scale bars: 20 pA/100ms.

(B) mEPSC frequency, but not IPSC amplitude, was lower in C4-OE mice (n = 16 cells from 6 mice) than in control mice (n = 20 cells from 3 mice; frequency: Mann-Whitney test, * P = 0.0184).

(C) Average of 12 consecutive recordings; EPSCs were evoked by paired-pulse stimulation and recorded in PV interneurons from control and C4-OE mice at a holding potential of -65 mV; scale bars: 50 pA/50 ms.

(D) Summary histogram of the paired-pulse ratio in control and C4-OE (control: n = 24 cells from 4 mice; C4-OE: n = 21 cells from 3 mice).

(E) Sample traces of mIPSCs recorded at a holding potential of −65 mV with a high-chloride intracellular solution in PV interneurons from control and C4-OE juvenile (P25-P30) mice, in the presence of TTX, APV and CNQX; scale bar: 20 pA/100 ms.

(F) Mean frequency (left) and amplitude (right) of mIPSCs in control (n = 18 cells from 4 mice) and C4-OE neurons (n = 13 cells from 4 mice).

All data are represented as mean ± SEM. Open circles represent single cells.

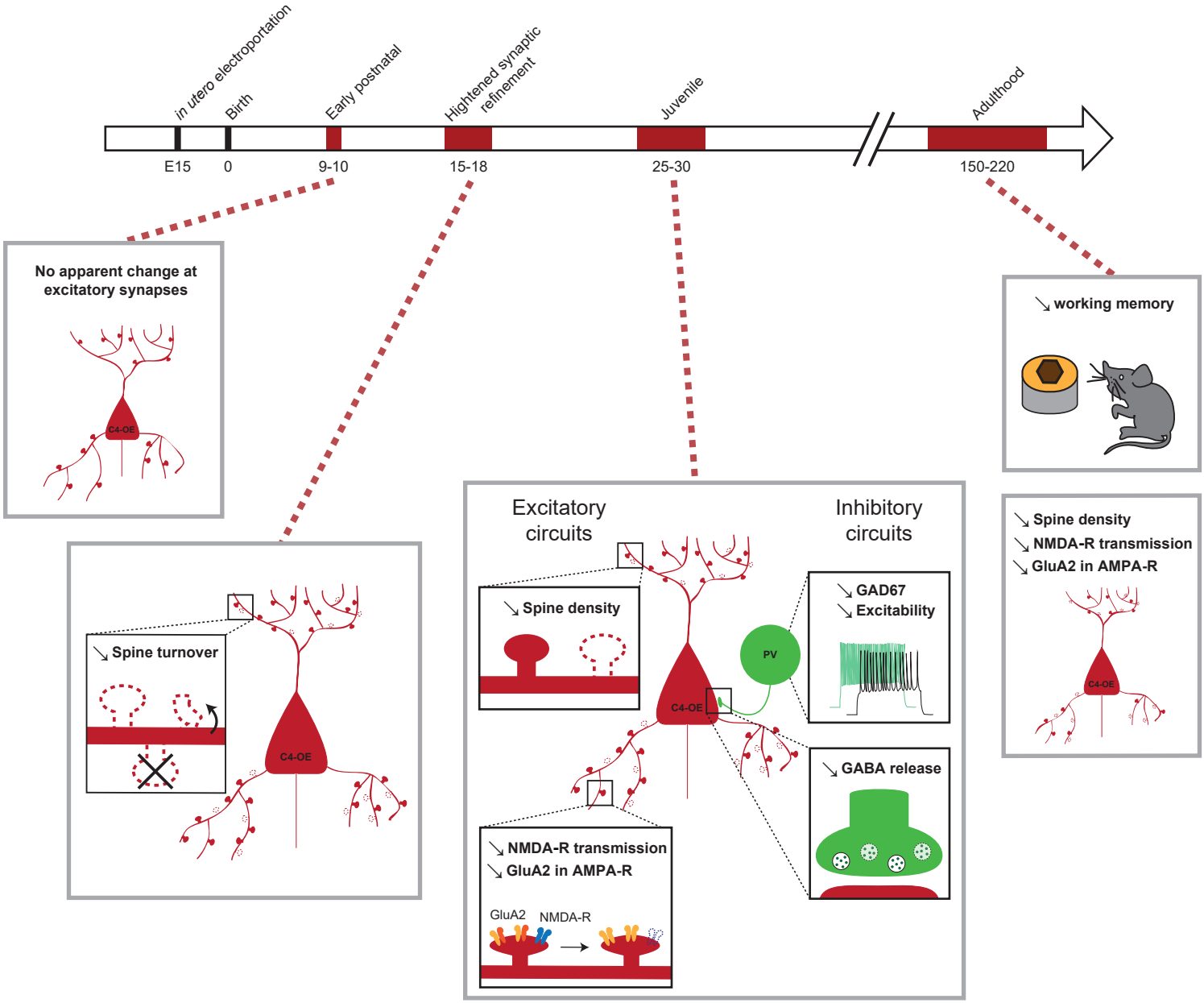

Supplementary Figure 8: Overview diagram summarizing the main findings at different stages of postnatal development

Table S1

	Control	n	N	L	C4-OE	n	N	L	Test	p value	Significant	F statistics (ANOVA)
Intrinsic properties at P25-P30												
Membrane resistance (MΩ)	91.9 ± 4.97	20	3	2	98.6 ± 7.62	17	3	3	T-test	0.456	ns	
Resting membrane potential (mV)	-70.9 ± 1.16	20	3	2	-71.2 ± 1.17	17	3	3	T-test	0.841	ns	
Membrane capacitance (pF)	327 ± 24.7	20	3	2	315 ± 31.6	17	3	3	T-test	0.773	ns	
Firing frequency		20	3	2		17	3	3	Two-way RM ANOVA	0.304	ns	$F_{(1,35)} = 1.09$
mEPSC frequency (Hz)									Two-way ANOVA	C4 factor: <0.0001	****	$F_{(1,105)} = 17.4$
										Age factor: <0.0001	****	$F_{(2,105)} = 54.4$
										Interaction: 0.0059	**	$F_{(2,105)} = 5.4$
P9-P10	2.03 ± 0.17	21	3	2	2.02 ± 0.15	18	4	2	Sidak's post-hoc test		ns	
P25-P30	10.2 ± 1.31	16	5	4	6.20 ± 0.90	14	6	3	Sidak's post-hoc test		####	
P150-P220	4.58 ± 0.36	20	6	4	2.59 ± 0.21	22	5	4	Sidak's post-hoc test		#	
Control: P9-P10 vs P25-P30									Sidak's post-hoc test		####	
Control: P25-P30 vs P150-P220									Sidak's post-hoc test		####	
Control: P9-P10 vs P150-P220									Sidak's post-hoc test		##	
C4-OE: P9-P10 vs P25-P30									Sidak's post-hoc test		####	
C4-OE: P25-P30 vs P150-P220									Sidak's post-hoc test		###	
C4-OE: P9-P10 vs P150-P220									Sidak's post-hoc test		ns	
mEPSC amplitude (pA)									Two-way ANOVA	C4 factor: 0.399	ns	$F_{(1,105)} = 0.716$
										Age factor: <0.0001	****	$F_{(2,105)} = 85.82$
										Interaction: 0.477	ns	$F_{(2,105)} = 0.745$
P9-P10	17.2 ± 1.241	21	3	2	17.7 ± 0.855	18	4	2	Sidak's post-hoc test		ns	
P25-P30	8.87 ± 0.586	16	5	4	8.10 ± 0.478	14	6	3	Sidak's post-hoc test		ns	
P150-P220	9.927 ± 0.442	20	6	4	8.637 ± 0.350	22	5	4	Sidak's post-hoc test		ns	
Control: P9-P10 vs P25-P30									Sidak's post-hoc test		####	
Control: P25-P30 vs P150-P220									Sidak's post-hoc test		ns	
Control: P9-P10 vs P150-P220									Sidak's post-hoc test		####	
C4-OE: P9-P10 vs P25-P30									Sidak's post-hoc test		####	
C4-OE: P25-P30 vs P150-P220									Sidak's post-hoc test		ns	
C4-OE: P9-P10 vs P150-P220									Sidak's post-hoc test		####	
Excitatory PPR									Two-way ANOVA	C4 factor: 0.809	ns	$F_{(1,105)} = 0.033$
										Age factor: 0.0011	**	$F_{(1,105)} = 7.31$
										Interaction: 0.806	ns	$F_{(1,105)} = 0.213$
P9-P10	0.916 ± 0.056	16	3	2	0.875 ± 0.031	21	3	2	Sidak's post-hoc test		ns	
P25-P30	1.04 ± 0.04	17	3	2	1.04 ± 0.05	21	3	2	Sidak's post-hoc test		ns	

P150-P220	1.06 ± 0.07	19	5	3	1.08 ± 0.04	17	4	3	Sidak's post-hoc test		ns	
Control: P9-P10 vs P25-P30									Sidak's post-hoc test		ns	
Control: P25-P30 vs P150-P220									Sidak's post-hoc test		ns	
Control: P9-P10 vs P150-P220									Sidak's post-hoc test		ns	
C4-OE: P9-P10 vs P25-P30									Sidak's post-hoc test		ns	
C4-OE: P25-P30 vs P150-P220									Sidak's post-hoc test		ns	
C4-OE: P9-P10 vs P150-P220									Sidak's post-hoc test		#	
AMPA/NMDA ratio									Two-way ANOVA	C4 factor: <0.0001	****	$F_{(1, 108)} = 18.9$
										Age factor: <0.0001	****	$F_{(2, 108)} = 40.6$
										Interaction: 0.007	**	$F_{(1, 108)} = 5.2$
P9-P10	0.856 ± 0.078	17	3	2	0.844 ± 0.085	21	3	2	Sidak's post-hoc test		ns	
P25-P30	0.928 ± 0.028	23	4	2	1.294 ± 0.086	20	5	3	Sidak's post-hoc test		###	
P150-P220	1.317 ± 0.073	17	4	2	1.752 ± 0.085	16	4	3	Sidak's post-hoc test		###	
Control: P9-P10 vs P25-P30									Sidak's post-hoc test		ns	
Control: P25-P30 vs P150-P220									Sidak's post-hoc test		###	
Control: P9-P10 vs P150-P220									Sidak's post-hoc test		###	
C4-OE: P9-P10 vs P25-P30									Sidak's post-hoc test		####	
C4-OE: P25-P30 vs P150-P220									Sidak's post-hoc test		###	
C4-OE: P9-P10 vs P150-P220									Sidak's post-hoc test		####	
NMDA decay time (ms)									Two-way ANOVA	C4 factor: 0.490	ns	$F_{(1, 108)} = 0.48$
										Age factor: <0.0001	****	$F_{(2, 108)} = 73.09$
										Interaction: 0.332	ns	$F_{(1, 108)} = 1.12$
P9-P10	0.098 ± 0.008	17	3	2	0.104 ± 0.006	21	3	2	Sidak's post-hoc test		ns	
P25-P30	0.056 ± 0.003	23	4	2	0.051 ± 0.002	20	5	3	Sidak's post-hoc test		ns	
P150-P220	0.058 ± 0.003	17	4	2	0.050 ± 0.002	16	4	3	Sidak's post-hoc test		ns	
Control: P9-P10 vs P25-P30									Sidak's post-hoc test		####	
Control: P25-P30 vs P150-P220									Sidak's post-hoc test		ns	
Control: P9-P10 vs P150-P220									Sidak's post-hoc test		####	
C4-OE: P9-P10 vs P25-P30									Sidak's post-hoc test		####	
C4-OE: P25-P30 vs P150-P220									Sidak's post-hoc test		ns	
C4-OE: P9-P10 vs P150-P220									Sidak's post-hoc test		####	
Rectification Index									Two-way ANOVA	C4 factor: <0.0001	****	$F_{(1, 112)} = 18.09$
										Age factor: 0.0058	**	$F_{(2, 112)} = 5.40$
										Interaction: 0.196	ns	$F_{(2,112)} = 1.65$
P9-P10	1.09 ± 0.06	20	3	2	1.02 ± 0.05	20	3	2	Sidak's post-hoc test		ns	
P25-P30	1.31 ± 0.05	21	3	3	1.06 ± 0.05	16	3	2	Sidak's post-hoc test		##	

P150-P220	1.13 ± 0.03	17	4	2	0.97 ± 0.03	24	3	2	Sidak's post-hoc test		#	
Control: P9-P10 vs P25-P30									Sidak's post-hoc test		##	
Control: P25-P30 vs P150-P220									Sidak's post-hoc test		#	
Control: P9-P10 vs P150-P220									Sidak's post-hoc test		ns	
C4-OE: P9-P10 vs P25-P30									Sidak's post-hoc test		ns	
C4-OE: P25-P30 vs P150-P220									Sidak's post-hoc test		ns	
C4-OE: P9-P10 vs P150-P220									Sidak's post-hoc test		ns	
mIPSC Amplitude at P25-P30 (pA)	17.1 ± 0.98	16	4	2	12.74 ± 0.46	16	6	4	T-test	0.0003	***	
mIPSC Frequency at P25-P30 (Hz)	7.08 ± 0.57	16	4	2	4.46 ± 0.61	16	6	4	Mann-Whitney test	0.0004	***	
Short-term plasticity of evoked IPSCs at P25-P30 (electrical stim)									Two-way RM ANOVA	0.089	ns	$F_{(1,64)} = 2.988$
Pulse II/ pulse I	0.542 ± 0.028	29	3	2	0.610 ± 0.027	37	3	2	Sidak's post-hoc test		ns	
Pulse III/ pulse I	0.437 ± 0.025	29	3	2	0.488 ± 0.024	37	3	2	Sidak's post-hoc test		ns	
Pulse IV/ pulse I	0.397 ± 0.022	29	3	2	0.442 ± 0.021	37	3	2	Sidak's post-hoc test		ns	
Short-term plasticity of evoked IPSCs at P25-P30 (optogenetics)									Two-way RM ANOVA	0.014	*	$F_{(1,71)} = 6.85$
Pulse II/ pulse I	0.541 ± 0.016	43	4	3	0.592 ± 0.021	30	3	2	Sidak's post-hoc test		ns	
Pulse III/ pulse I	0.400 ± 0.013	43	4	3	0.465 ± 0.019	30	3	2	Sidak's post-hoc test		#	
Pulse IV/ pulse I	0.357 ± 0.014	43	4	3	0.411 ± 0.018	30	3	2	Sidak's post-hoc test		ns	

Table S1. Summary table of patch-clamp results (pyramidal cells)

N refers to the number of mice, n refers to the number of neuronal recordings, L refers to the number of litters. All data are presented as mean ± SEM. Sidak's test # $P < 0.05$; ## $P < 0.01$; ### $P < 0.001$; #### $P < 0.0001$.

Table S2

	Control	N	L	C4-OE	N	L	Test	p value	Significant	F statistics (ANOVA)
***In vivo* 2-photon imaging at P30**										
Spine density	0.880 ± 0.043	10	3	0.666 ± 0.029	7	3	T-test	0.0023	**	
***In vivo* 2-photon imaging at P15-P18**										
Spine density at 0h	1.145 ± 0.028	5	3	0.921± 0.021	7	3	Mann-Whitney test	0.0025	**	
Spine density from 0h to 4h		5	3		7	3	Two-way RM ANOVA	C4 factor: < 0.0001	****	$F_{(1,10)} = 44.8$
								Time factor: 0.780	ns	$F_{(1,10)} = 0.083$
								Interaction 0.366	ns	$F_{(1,10)} = 0.899$
Stable spine density	1.044 ± 0.024	5	3	0.883 ± 0.002	7	3	T-test	0.0007	***	
Gained spine density	0.092 ± 0.009	5	3	0.045 ± 0.007	7	3	T-test	0.0018	**	
Lost spine density	0.099 ± 0.006	5	3	0.039 ± 0.006	7	3	T-test	< 0.0001	****	
Turnover rate (%)	8.767 ± 0.545	5	3	5.091 ± 0.728	7	3	T-test	0.0039	**	
Fixed tissue at P15-P18										
Spine density	1.731 ± 0.035	7	3	1.541 ± 0.061	8	3	T-test	0.023	*	
GAD 67 expression										
Mean intensity (% control group)	100 ± 3.36	28	9	86.62 ± 3.59	33	10	T-test	0.0094	**	
PV cell distribution		9	3		10	3	Two-way ANOVA	0.563	ns	$F_{(1,68)} = 0.338$
Layer II/III	21.1 ± 1.4	9	3	20.4 ± 1.9	10	3	Sidak's post-hoc test		ns	
Layer IV	31.1 ± 2.3	9	3	29.5 ± 2.0	10	3	Sidak's post-hoc test		ns	
Layer V	33.8 ± 2.5	9	3	33.4 ± 1.5	10	3	Sidak's post-hoc test		ns	
Layer VI	11.8 ± 1.2	9	3	11.5 ± 1.0	10	3	Sidak's post-hoc test		ns	
PV cell total number	24.4 ± 1.5	9	3	23.7 ± 1.21	10	3	T-test	0.705	ns	

Table S2. Summary table of imaging results

N refers to the number of mice, L refers to the number of litters. All data are presented as mean ± SEM.

Table S3

	Control	n	N	L	C4-OE	n	N	L	Test	p value	Significant	F statistics (ANOVA)
Intrinsic properties												
Membrane resistance (MΩ)	129.4 ± 8.8	20	3	2	98.3 ± 7.0	21	4	2	Mann-Whitney test	0.0024	**	
Resting membrane potential (mV)	-68.0 ± 0.8	20	3	2	-68.6 ± 0.8	21	4	2	T-test	0.881	ns	
Membrane capacitance (pF)	151 ± 15	20	3	2	124 ± 14	21	4	2	Mann-Whitney test	0.127	ns	
Firing		20	3	2		21	4	2	Two-way ANOVA	C4 factor: 0.0129	*	$F_{(1,37)} = 6.82$
										Depolarization: <0.0001	****	$F_{(10,370)} = 371.8$
										Interaction: <0.0001	****	$F_{(10,370)} = 4.17$
mEPSC Amplitude (pA)	13.8 ± 0.7	18	5	3	15.1 ± 0.6	16	6	3	Mann-Whitney test	0.069	ns	
mEPSC Frequency (Hz)	17.9 ± 1.4	18	5	3	27.9 ± 3.1	16	6	3	Mann-Whitney test	0.018	*	
Excitatory PPR	1.04 ± 0.06	24	4	2	1.12 ± 0.05	21	3	2	T-test	0.251	ns	
mIPSC Amplitude (pA)	13.9 ± 0.8	18	4	2	15.4 ± 1.4	13	4	3	T-test	0.312	ns	
mIPSC Frequency (Hz)	9.25 ± 0.97	18	4	2	10.8 ± 1.43	13	4	3	T-test	0.365	ns	

Table S3. Summary table of patch-clamp results (PV interneurons)

N refers to the number of mice, n refers to the number of neuronal recordings, L refers to the number of litters. All data are presented as mean ± SEM.

Table S4

	Control	N	L	C4-OE	N	L	Test	p value	Significant	F statistics (ANOVA)
Locomotion										
Actimeter (repeated measures)		32	12		21	9	Two-way RM ANOVA	C4 factor: 0.765	ns	$F_{(1,51)} = 0.09$
								Time factor: < 0.0001	****	$F_{(11,561)} = 31.82$
								Interaction 0.366	ns	$F_{(11,561)} = 0.584$
Actimeter total activity	384 ± 21	32	12	396 ± 38	21	9	Mann-Whitney test	0.531	ns	
Open field (repeated measures)		20	10		14	8	Two-way RM ANOVA	C4 factor: 0.127	ns	$F_{(1,32)} = 2.458$
								Time factor: < 0.0001	****	$F_{(8,256)} = 4.250$
								Interaction 0.0037	**	$F_{(8,256)} = 2.975$
Open field total activity	2242 ± 121	20	10	1950 ± 140	14	8	Mann-Whitney test	0.189	ns	
Working memory										
Non-matching to sample		15	5		14	6	Two-way RM ANOVA	C4 factor: 0.556	ns	$F_{(1,135)} = 0.348$
								Time factor: < 0.0001	****	$F_{(1,135)} = 51.80$
								Interaction 0.364	ns	$F_{(4,135)} = 0.364$
Odor Span	8.40 ± 0.83	15	5	4.43 ± 0.54	14	6	Mann-Whitney test	0.0022	**	
Spatial Span	6.40 ± 0.73	15	4	4.21 ± 0.68	14	6	Mann-Whitney test	0.045	*	

Table S4. Summary table of behavioral studies

N refers to the number of mice, L refers to the number of litters. All data are presented as mean ± SEM.